Monthly Notices of the ROYAL ASTRONOMICAL SOCIETY

MNRAS **497,** 5518–5539 (2020) doi:10.1093/mnras/staa1846
Advance Access publication 2020 June 26

GRANDMA observations of advanced LIGO's and advanced Virgo's third observational campaign

S. Antier[1★] S. Agayeva,[2] M. Almualla,[3] S. Awiphan,[4] A. Baransky,[5,6] K. Barynova,[5,6] S. Beradze,[7,8] M. Blažek[9] M. Boër[10] O. Burkhonov,[11] N. Christensen,[10] A. Coleiro,[1] D. Corre,[12] M. W. Coughlin[13] H. Crisp,[14] T. Dietrich,[15] J.-G. Ducoin,[12] P.-A. Duverne,[12] G. Marchal-Duval,[12] B. Gendre[14] P. Gokuldass,[16] H. B. Eggenstein,[17] L. Eymar,[10] P. Hello,[12] E. J. Howell[14] N. Ismailov,[2] D. A. Kann,[9] S. Karpov,[18] A. Klotz,[19,20] N. Kochiashvili,[7] C. Lachaud,[1] N. Leroy,[12] W. L. Lin,[21] W. X. Li,[21] M. Mašek,[18] J. Mo,[21] R. Menard,[1] D. Morris,[16] K. Noysena,[19,20] N. B. Orange,[22] M. Prouza,[18] R. Rattanamala,[23] T. Sadibekova,[11,24] D. Saint-Gelais,[1] M. Serrau,[1] A. Simon,[25] C. Stachie,[10] C. C. Thöne,[9] Y. Tillayev,[11,26] D. Turpin[24] A. de Ugarte Postigo,[9] V. Vasylenko,[25] Z. Vidadi,[2] M. Was,[27] X. F. Wang,[21] J. J. Zhang,[28] T. M. Zhang[29] and X. H. Zhang[21]

Affiliations are listed at the end of the paper

Accepted 2020 June 19. Received 2020 June 17; in original form 2020 April 14

ABSTRACT

GRANDMA (Global Rapid Advanced Network Devoted to the Multi-messenger Addicts) is a network of 25 telescopes of different sizes, including both photometric and spectroscopic facilities. The network aims to coordinate follow-up observations of gravitational-wave (GW) candidate alerts, especially those with large localization uncertainties, to reduce the delay between the initial detection and the optical confirmation. In this paper, we detail GRANDMA's observational performance during Advanced LIGO/Advanced Virgo Observing Run 3 (O3), focusing on the second part of O3; this includes summary statistics pertaining to coverage and possible astrophysical origin of the candidates. To do so, we quantify our observation efficiency in terms of delay between GW candidate trigger time, observations, and the total coverage. Using an optimized and robust coordination system, GRANDMA followed-up about 90 per cent of the GW candidate alerts, that is 49 out of 56 candidates. This led to coverage of over 9000 deg^2 during O3. The delay between the GW candidate trigger and the first observation was below 1.5 h for 50 per cent of the alerts. We did not detect any electromagnetic counterparts to the GW candidates during O3, likely due to the very large localization areas (on average thousands of degrees squares) and relatively large distance of the candidates (above 200 Mpc for 60 per cent of binary neutron star, BNS candidates). We derive constraints on potential kilonova properties for two potential BNS coalescences (GW190425 and S200213t), assuming that the events' locations were imaged.

Key words: gravitational waves – methods: observational – stars: neutron.

1 INTRODUCTION

Gravitational-wave (GW) signals detected by Advanced LIGO (Aasi et al 2015) and Advanced Virgo (Acernese et al 2015) since 2015 have revealed the existence of compact binary mergers which included neutrons stars (NSs, Abbott et al. 2017a, 2020a) and black holes (BHs, Abbott et al. 2019e), providing unprecedented new insights into these objects.

During the first and second Advanced LIGO and Advanced Virgo observing runs, O1 and O2 (2015–2017, Advanced Virgo joined at the end of O2), GWs from 10 binary BH (BBH) systems and a binary NS system (BNS) were detected (Abbott et al. 2017a, 2019e). Additional events produced by BBHs were also claimed by other groups analysing the LIGO/Virgo data (Zackay et al. 2019). The GW observations of these compact binary sources have allowed gravity to be probed in the ultrastrong field regime (Abbott et al. 2016), and have yielded new ideas on the formation channels of the systems (Abbott et al. 2019b).

The first GW observation from a coalescing BNS, GW170817 (Abbott et al. 2017a) and the joint observations of GRB 170817A by the *Fermi*/GBM and *INTEGRAL*/SPI ACS gamma-ray detectors (Goldstein et al. 2017; Savchenko et al. 2017) firmly established the association between BNS mergers and short-duration gamma-ray bursts (GRBs). The estimation of the source location of GW170817 and its subsequent identification at a distance of 40 Mpc (Coulter et al. 2017) initiated a ground-breaking electromagnetic (EM) follow-up campaign from the X-ray to radio bands. These EM observations provided evidence that a successful jet was launched and that the initial gamma-ray emission were from a structured jet viewed approximately 20° off-axis (Mooley et al. 2018; Ghirlanda et al. 2019).

★ E-mail: antier@apc.in2p3.fr

Furthermore, optical, ultraviolet, and infrared observations of the optical counterpart AT 2017gfo (Coulter et al. 2017) monitored the glow of a 'kilonova,' produced by the radioactive decay of *r*-process elements in the neutron-rich ejecta (Lattimer & Schramm 1974; Li & Paczynski 1998; Kasen et al. 2017) and showed that the source evolved from blue to red over a week (Abbott et al. 2017b; Arcavi 2018). The impact of this discovery motivated a large number of small aperture telescopes to systematically scan the credible regions provided by LIGO/Virgo GW candidate event triggers during subsequent LIGO/Virgo observational runs. The most recent run, O3, which began in 2019 April, was split into two parts to allow for a commissioning break: O3a (2019 April–2019 September) and O3b (2019 November–2020 March 27; somewhat more than a month earlier than planned because of the COVID-19 pandemic).

Since the discovery of the EM counterpart of GW170817 no other counterpart associated with a GW candidate event has been observed despite significant coordinated efforts by numerous observing groups, for example Coughlin et al. (2019c), Hosseinzadeh et al. (2019), Goldstein et al. (2019), Andreoni et al. (2020a), Ackley et al. (2020), and Brunn et al. (2019).

The potential BNS sources[1] reported so far by the LIGO/Virgo network in O3 (a sample of five with a BNS source probability of $>$ 50 per cent) have median estimated distances in the range $\sim$157–241 Mpc with only one source, GW190425 (Abbott et al. 2020), within 200 Mpc.

Additionally, the 90 per cent confidence intervals of the sky localizations for this sample cover the range 1131–24226 deg^2. The combination of large credible regions coupled with the dimmer optical counterparts expected at such large distances have made searches for EM counterparts a highly challenging (and ultimately unsuccessful) endeavour during O3.

When conducting searches of large GW sky localizations with a single instrument, a telescope with a large field of view (FoV) is optimal. However, there is a delicate balance; large credible regions are often the result of more distant sources observed at relatively lower signal-to-noise ratio (S/N) – but sources at greater distances are more accessible to larger diameter telescopes. It is both technically and financially challenging to have a large aperture telescope capable of covering a large FoV. This has motivated the use of multiple telescopes working in unison within global networks for the purpose of identification and characterization of counterparts; see, for example Coughlin et al. (2020b). In addition to GRANDMA (Global Rapid Advanced Network Devoted to the Multi-messenger Addicts), the heterogeneous telescope network described in this paper, other networks such as the Global Relay of Observatories Watching Transients Happen (GROWTH, Coughlin et al. 2019c), MASTER-Net (Lipunov et al. 2010), and KMTNet[2] have also been conducting counterpart searches during O3, supported by a host of individual facilities such as Pan-STARRS1 (Flewelling et al. 2016), ATLAS (Tonry 2011), DECam (Herner et al. 2017), MeerLICHT (Bloemen et al. 2016), DDOTI (Watson et al. 2020), and GOTO[3] (O'Brien 2018). The O3 campaign has also seen the emergence of a variety of new tools and multimessenger platforms to coordinate and optimize the follow-up: galaxy ranking can be optimized through the online catalogue MANGROVE (Ducoin et al. 2020a); the GWEMOPT open software can be used to schedule GW follow-ups (Coughlin et al. 2018a); and the GW TreasureMap (Wyatt et al. 2020) is a system to report and visualize the progress of searches for EM counterparts to GW events.

In a previous paper (Antier et al. 2020), we published the GRANDMA results obtained during O3a. This current paper continues in a similar vein through the study of candidate events from O3b. The paper is organized as follows: Section 2 outlines the GW candidate alerts received during O3, and Section 3 describes the new telescopes that joined the GRANDMA collaboration for O3b. Section 4 provides details on the adopted observational strategies. Section 5 presents details on the GRANDMA observations, focuses on some specific events, and provides new constraints on the GW progenitors. We finish by presenting our conclusions in Section 6.

2 OVERVIEW ON THE THIRD OBSERVATIONAL CAMPAIGN O3

The third observational campaign organized by LIGO and Virgo, O3, started 2019 April 1 at 15:00 UTC (LIGO Scientific Collaboration & Virgo Collaboration 2019a). After a month-long commissioning break in October, the second period of the campaign finished on 2020 March 27 at 17:00 UTC, for a total of 330 d, short of the goal of a full 365 d, cut short by the COVID-19 pandemic. For comparison, the second observational campaign lasted 269 d and the first observational campaign lasted 129 d (Veitch et al. 2015).

2.1 O3 alerts

During O3, the LIGO Scientific Collaboration and the VIRGO Collaboration (LVC) sent 80 alerts to the astronomical community (and about 100 in total for the O1, O2, and O3 observational campaigns combined). Among them, 24 were false positives resulting in retractions due to data quality issues (see for instance LIGO Scientific Collaboration & Virgo Collaboration 2019p, 2020b, f) and 56 are still considered as potential signals. 52 were classified as GW signals with a probability higher than 50 per cent[4] via the GCN platform (Gamma-ray burst Coordinates Network[5]) thanks to a new dedicated alert system developed by the LVC.[6] The alert system was still being debugged for the first two months (April and May), producing a large delay of dozens of minutes between the alert delivery and the GW trigger time (the event UTC time). The delay was typically less than 10 min for the remainder of the run, although some exceptional delays did occur for non-technical reasons, that is S200219ac (LIGO Scientific Collaboration & Virgo Collaboration 2020j), S200105ae (LIGO Scientific Collaboration & Virgo Collaboration 2020a), and S191105ae (LIGO Scientific Collaboration & Virgo Collaboration 2019n) during O3b.

The GW alerts were distributed with three different types of GCN/LVC notices with different distribution delays: preliminary (within 5 min), initial (within 30 min, produced after human vetting), and update notices (within 2–4 d, produced after a refined parameter estimation analysis). The notices contain information such as the trigger time, the online pipeline that generated the trigger, the event false alarm rate, a link to the sky localization probability map (Bayestar, Singer & Price 2016 or LALInference, Veitch et al.

[1]Note that we make the assumption in this paper that any compact object component with mass $<3\,M_\odot$ is an NS.
[2]https://kmtnet.kasi.re.kr/kmtnet-eng/
[3]Currently operating with one operational site, with funding approved for an additional node in Australia.

[4]See https://gracedb.ligo.org/superevents/public/O3/ for more information.
[5]See https://gcn.gsfc.nasa.gov/ for more information
[6]See the LIGO/Virgo userguide for more information https://emfollow.docs.ligo.org/userguide/

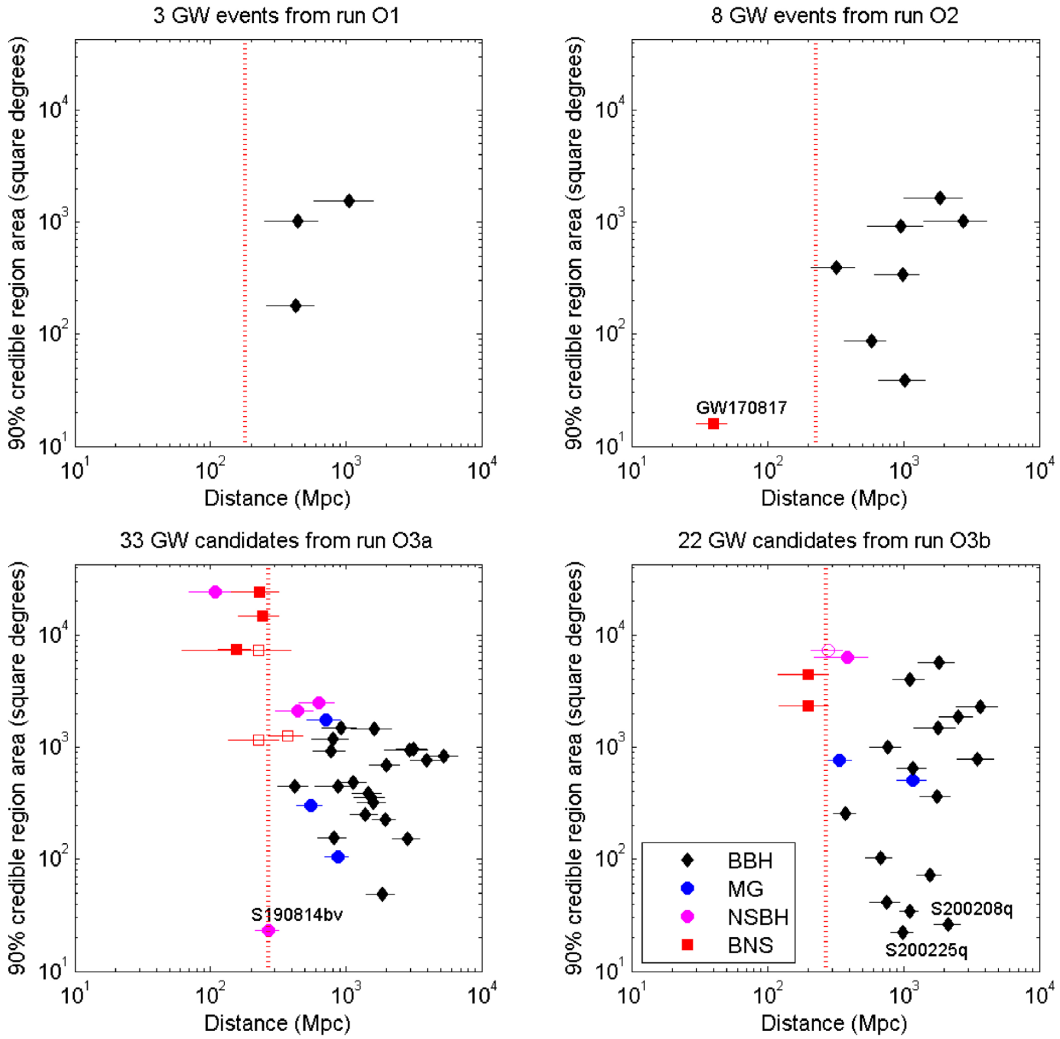

Figure 1. The most recently updated 90 per cent credible region area versus the most recently updated luminosity distance (posterior mean distance and posterior standard deviation of distance) for all LIGO/Virgo GW events/candidates of runs O1, O2, O3a, and O3b. Vertical red dotted lines are the expected limiting distances to detect BNS mergers by the LIGO/Virgo detectors. BBH, MG, and NSBH are represented in different colours. Four candidates for run O3 are indicated by open symbols corresponding to a predominantly terrestrial classification (above 50 per cent) and the classification indicated in these plots is the second most likely.

2015), and the estimate of the distance to the source. The alert also contains different source classification information if available for compact binary searches: a BNS [p(BNS)], a BHNS [p(BHNS)], or terrestrial noise [p(terrestrial)] (Kapadia et al. 2020), and an indicator to estimate the probability of producing an EM signature considering the candidate is of astrophysical origin [p(HasRemnant)] (Chatterjee et al. 2019). The GW trigger can be also classified as 'MassGap,' completing the possible classifications. In the case of a Mass Gap event, the initial estimate is that at least one of the compact objects has a mass of 3–5 $M_{\odot}$, implying it is unclear whether it is an NS or a BH. The other object can be a lighter NS or a more massive BH. Up to the time when this paper was written, only the 'superevent' S190425z has been confirmed as a real astrophysically produced GW event, GW190425 (Abbott et al. 2020).

Out of the 52 GW candidates detected in O3, 36 have been classified as likely being emitted from a BBH merger, five from mass gap mergers, five from BHNS mergers, five from BNS mergers, and one was a GW 'burst' type trigger (unmodelled search) of unidentified origin (LIGO Scientific Collaboration & Virgo Collaboration 2020d; Klimenko et al. 2016). Except for the case of the burst GW signal, the rest have information on their distance derived from the GW binary coalescence signal modelling. The final event classification can differ from the low latency analysis due to the further study subsequently conducted. This is especially the case for low-mass binaries with one object close to the lower or upper bound of the 3–5 $M_{\odot}$ gap that can be reclassified 'NSBH', 'BBH', or 'Mass Gap': S190814bv was given a final classification of 99 per cent 'NSBH' (LIGO Scientific Collaboration & Virgo Collaboration 2019j, k), and S190728q as 52 per cent Mass Gap (LIGO Scientific Collaboration & Virgo Collaboration 2019h, i). In addition, the indication regarding probability to be of astrophysical origin has also evolved for some of the GW candidates: S190426c and S190510g now have a preferential origin of being 'Terrestrial' (LIGO Scientific Collaboration & Virgo Collaboration 2019b, c, l); on the contrary, S190727h is now considered as an astrophysical event with 92 per cent 'BBH' (LIGO Scientific Collaboration & Virgo Collaboration 2019g); S200105ae is still classified as 97 per cent 'Terrestrial' but the LVC reported that the low false alarm rate for this

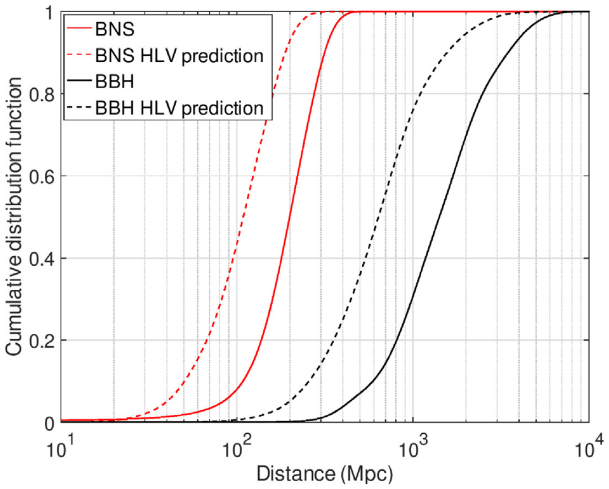

Figure 2. The cumulative distribution function of all LIGO/Virgo GW events and candidates in O3 with a Terrestrial indicator below 50 per cent versus the distance is shown in solid lines, compared to the predictions for these distribution from Abbott et al. (2018a) shown in dashed lines.

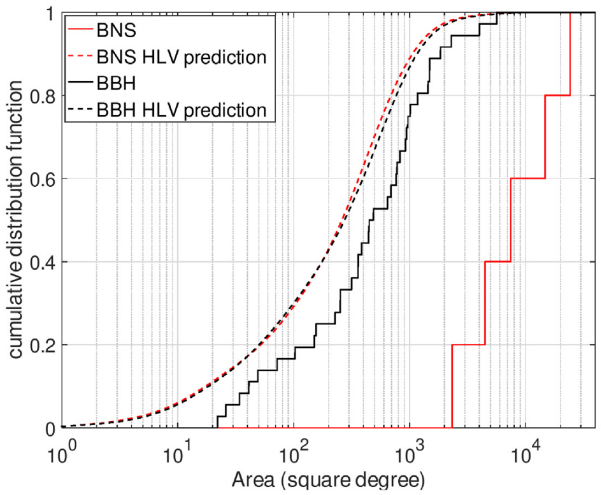

Figure 3. The cumulative distribution function of all LIGO/Virgo GW events and candidates in O3 with a Terrestrial indicator below 50 per cent versus the 90 per cent credible localization area is shown in solid lines, compared to the predictions for these distributions from Abbott et al. (2018a) shown in dashed lines.

trigger was due to only one detector (LIGO Livingston) responding to the event and offline analysis is likely to increase its significance (LIGO Scientific Collaboration & Virgo Collaboration 2020a, c).

The localization area for GW alerts also differs from the initial to the updated analysis for some events (e.g. due to the inclusion of Virgo data in the analysis for S200225q, LIGO Scientific Collaboration & Virgo Collaboration 2020k). These issues will be discussed in Section 2.2. Note that the reports for the distance estimate can also vary (e.g. S200219ac, LIGO Scientific Collaboration & Virgo Collaboration 2020j), but we will not discuss this distance analysis in this paper.

Fig. 1 displays the most recently issued 90 per cent credible localization region produced for a GW candidate versus its most recently updated luminosity distance (posterior mean distance and posterior standard deviation of distance): all detailed numbers can be found in Antier et al. (2020) for O3a and Section 5 for O3b. We split the diagram into four sections, one for each of the O1, O2, O3a, and O3b observational campaigns. We indicate the names of detected events and candidates if their error boxes are smaller than 30 deg^2 containing one confirmed BNS event (GW170817, Abbott et al. 2017a, 2019e), an NS–BH candidate (S190814bv, LIGO Scientific Collaboration & Virgo Collaboration 2019k), and two BBH candidate events (S200225q, LIGO Scientific Collaboration & Virgo Collaboration 2020k, and S200208q, LIGO Scientific Collaboration & Virgo Collaboration 2020g).

For each kind of event, a cumulative distribution function on the distance can be constructed by approximating each measured distance and error bar with a Gaussian function. The combined distribution is shown in Fig. 2, along with the predictions provided by the LVC (Abbott et al. 2018a). There is a clear separation between the BNS and BBH distributions. This is due to the much higher rate of BNS mergers compared to BBH mergers[7] (Abbott et al. 2019e), and to the much smaller distance at which BNS mergers can be detected by GW detectors compared to BBH mergers. Hence, BBH mergers are detected often at large distances where the large volume compensates for the low rate. In particular, there is no BBH candidate or event detected below 200 Mpc.

The observed distances are larger than the prediction by approximately a factor 2 for BNS and BBH event types. This could be due to the conservative detection threshold on network S/N of 12 used in the prediction described in Abbott et al. (2018a) and by masses for the binary system being larger than those used in the simulations. The study of this discrepancy is beyond the scope of this paper. In particular, the median distance of BNS candidates in the run O3 is 200 Mpc, 5 times further than GW170817. As a consequence, the apparent magnitudes of kilonovae associated with the BNS events of the run O3 are expected to be ∼3.5 mag fainter than for GW170817, assuming the same intrinsic light curve.

The 90 per cent credible region areas can be combined to obtain a cumulative distribution function for the localization area. This is shown in Fig. 3 and compared with the predictions provided by the LIGO/Virgo collaboration (Abbott et al. 2018a). For BBH mergers, the localization area is on average a factor 2 larger than predicted. Similar to the distance distribution, the difference could be due to larger masses and smaller network S/N of the signals detected as opposed to those from the simulations, as both properties are expected to reduce localization performance. For BNS mergers the discrepancy with the prediction is larger by a factor of 10. This is more difficult to explain, but we note that three out of eight BNS candidates have a significant probability (above 50 per cent) of being Terrestrial. GW190425 is the only confident detection from O3 announced by the LVC so far (Abbott et al. 2020), but it was observed by only two GW detectors and with a very low S/N in one of them, which explains its poor sky localization. In comparison with O2, the sky localization areas of the eight BNS candidates produced during the run O3 are spread over a median value of 4500 deg^2 (i.e. 10 per cent of the sky), 300 times larger than for GW170817, which was observed by three GW detectors.

The large GW alert rate in O3 provides motivation for a first estimate of the rate at which each classification of event (BNS, NS–BH, MassGap, and BBHs); see Abbott et al. (2018a, 2019e) for a discussion giving a more sophisticated approach. Our method is as follows: for each type of event we calculate the mean distance for

[7]The GWTC-1 catalogue gives 110–3840 events Gpc$^{-3}y^{-1}$ for BNSs and 9.7–101 events Gpc$^{-3}y^{-1}$ for BBHs.

Table 1. Statistics for each GW candidate/event source type during O3, see the main text for further details.

Type	Detections	Mean D_L (Mpc)	Volume (Gpc^3)	Rate (events yr^{-1} Gpc^{-3})
BNS	5	206	0.037	152
NS–BH	5	366	0.205	27
Mass gap	5	737	1.675	3.3
BBH	36	1649	18.77	2.1

which they are detected. Next, from this distance we can determine the enclosed volume that it represents, and estimate an event rate. To do this, we divide the number of GW candidates during the observational period by its duration, and divide that result by the volume determined for the type of event as presented in Table 1. A Monte Carlo study shows that this method yields, on average, the correct rate estimate if all events of the same type can be detected up to the same limiting distance (i.e. there is no large dispersion in the chirp masses). This is approximately true for BNS events, but for BBH systems there is a wide distribution in masses which will lead to a large systematic error (Abbott et al. 2019e). We cannot quantify this bias as the chirp mass of the systems are not yet publicly distributed.

2.2 Localization and observational constraints

In order to give insight into the O3 campaign, it is useful to quantify the possibility of observing during the nights following the detection, as well as the benefit of observing after the initial sky localization is released but before the updated sky localization is available. Due to factors such as high airmass and the Sun's altitude, the possibility of observing from a certain location may be different than others, and so it is important to take this into consideration when attempting to follow-up candidate events. Both initial and updated sky localization areas are available for 41 candidates. Fig. 4 displays the cumulative distribution function for the observable probability within the localization from three representative locations (Palomar, The Cerro Tololo Inter-American Observatory, and Hawaii) for all candidate events during O3. As can be seen in the figure, around 20 per cent of events were not observable at all from at least one of the three locations in the week following detection. We also find that a further ∼16 per cent of candidates had $\lessapprox$ 4 per cent of the probability observable from all three locations; all of these transients have 90 per cent credible regions spanning less than 300 deg^2 (except for S190602aq, LIGO Scientific Collaboration & Virgo Collaboration 2019d, for which it spans ∼750 deg^2) and were classified to very likely be BBH mergers (aside from S190924h, LIGO Scientific Collaboration & Virgo Collaboration 2019m, which was classified as a mass gap candidate at > 99 per cent). Additionally, 20 per cent of candidates had more than 40 per cent observability from only one of the three sites, demonstrating the utility of coordinating network-level telescope observations to obtain large coverage of the localizations. The importance of obtaining such observations at significant depth and coverage (regardless of whether an EM counterpart is ultimately discovered) cannot be overstated, as it has a direct impact on the ability to constrain the ejecta mass and binary parameters for the event if it is truly astrophysical in origin (Coughlin et al. 2020b).

Fig. 5 presents the distribution of the percent overlap between the 90 per cent credible regions of the initial Bayestar (Singer & Price 2016) and the updated LALInference (Veitch et al. 2015)

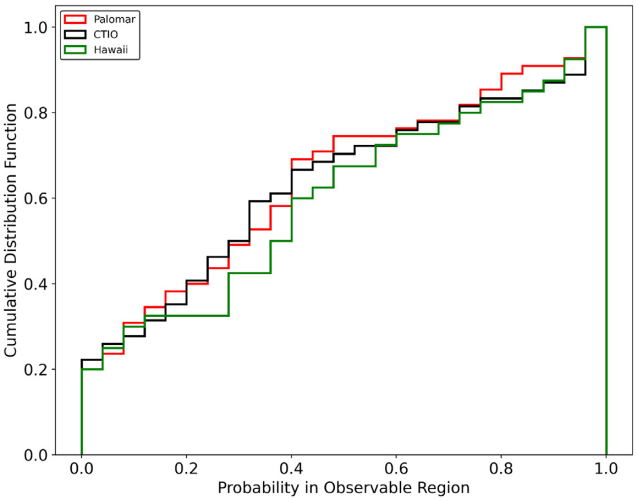

Figure 4. Probability contained within the observable region of the sky localization for all GW candidates during O3; this is shown from three different locations (Palomar (33.3563°, −116.8648°), CTIO (−30.1691°, −70.8062°), and Hawaii (19.8968°, 155.5828°); the LALInference sky localization was used as long as it was available for the candidate/event in question.

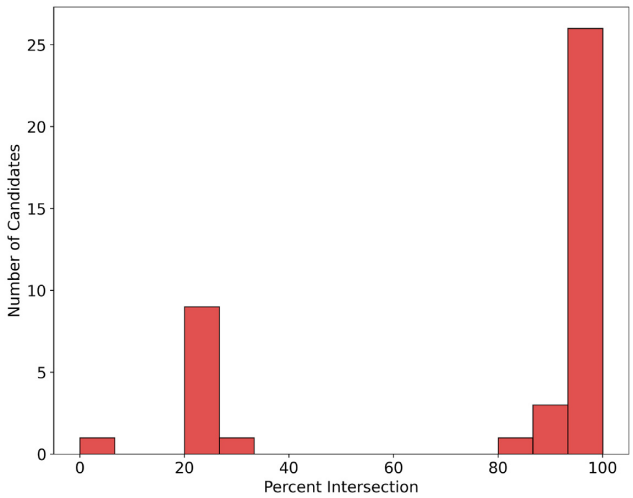

Figure 5. Overlap ratio between the initial and the most up-to-date 90 per cent credible regions of all GW candidate events during O3 (given that both sky localizations were available). Note that the overlapping regions can be discontinuous.

sky localization areas for 41 candidate events from O3. To find the percent overlap, we compute the intersection in pixels between the two maps and then sum the probability contained in that region using the LALInference sky area. From the results, we find that the events fall into one of two possible categories: a low percentage overlap (∼0–30 per cent) or a high percentage overlap (close to 100 per cent). Around 27 per cent of the events belong to the first category, showing that a significant number of candidates experience a large shift in their 2D probability distribution. This shift is likely due to a variety of factors. For one, some multi-instrument detections did not factor in data from one of the GW detectors when generating the initial Bayestar skymap (e.g. S190720a, LIGO Scientific Collaboration & Virgo Collaboration 2019f), and for other events, the sky area decreased significantly between the two sky

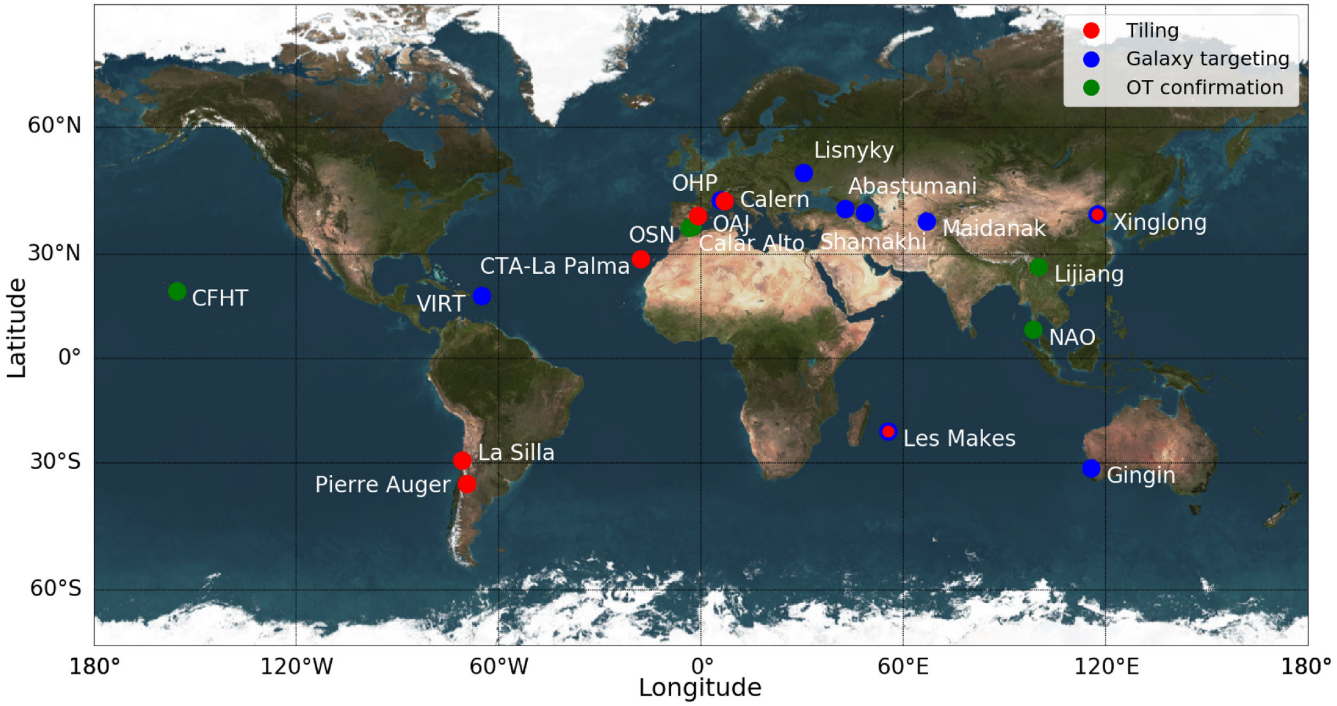

Figure 6. Locations of the 20 observatories involved in the GRANDMA network. The colour encodes the observation strategy followed by telescopes at a given observatory: *red* for tiling, *blue* for targeting galaxies, and *green* for following-up candidates.

localizations (e.g. S200225q, LIGO Scientific Collaboration & Virgo Collaboration 2020k, with the inclusion of Virgo, and S190630ag, LIGO Scientific Collaboration & Virgo Collaboration 2019e). In addition, disagreement between the time delays of the detected signals for the event and the results of the parameter estimation, as well as unanticipated issues (e.g. the occurrence of scattered light glitches in some of the detectors in the case of S191213g, LIGO Scientific Collaboration & Virgo Collaboration 2019o, which possibly affected the sky position) may have led to the low percentage overlap for some events.

3 UPDATE OF THE GRANDMA COLLABORATION

GRANDMA, a worldwide telescope network, was presented in Antier et al. (2020) in the context of O3a. Recently, new groups have joined the collaboration, as will be described below; also presented are updates on the observation strategies and results of certain subgroups. To date, GRANDMA is composed of 25 telescopes with both photometric and spectroscopic facilities, with a large amount of time allocated for observing transient alerts as a telescope network (see Fig. 6, and Tables 2 and 3). The GRANDMA collaboration includes 20 observatories, 29 institutions, and groups from 12 countries.

For each of the observatories we provide a 5σ limiting magnitude as an estimate of the faintness of sources that can be reliably discovered by our system. The 5σ limit is the usual choice of most astronomical surveys (SDSS, York et al. 2000; LSST, LSST Science Collaboration 2009; PanSTARRS, Chambers et al. 2016, etc.) as well as other GW follow-up efforts (e.g. GROWTH, Coughlin et al. 2019c, and GOTO, O'Brien 2018), and it implies that only one out of 1.7 million sources above this threshold would be a false detection. However, since in our case we are just looking for point-like sources in images with well-known point spread functions (PSFs), our system is capable of filtering out many of these sources (which do not have stellar PSFs) and significantly reducing the number of false positives. Our current neural network system (see Section 4) has shown to be able to reduce the number of false positives by a factor of several thousand. This makes the 5σ limit provided here a conservative one.

3.1 Canada–France–Hawaii Telescope

Twelve hours of observing time have been awarded (PI: A. Coleiro) on the Canada–France–Hawaii 3.6-m world-class telescope (CFHT) for period 2020A in order to trigger target-of-opportunity photometric observations. The telescope is located on top of the Mauna Kea summit in Hawaii and is equipped with two imaging instruments: a $1^\circ \times 1^\circ$ FoV optical camera, MegaCam, complemented by a 20 arcmin × 20 arcmin FoV near-infrared detector, WIRCam. By providing high-sensitivity and wide FoV optical (i', r', and z') and near-infrared (J, H, and K_s) data, CFHT is an essential element of the GRANDMA network, allowing for a fast identification of the EM counterpart and/or its physical characterization. To strengthen their scientific impact, we asked all data to be made freely available to the whole community when delivered to the GRANDMA team. However, due to the premature end of the scientific operations of both CFHT and the GW observatories at the end of 2020 March, no observations were triggered on CFHT during period 2020A.

3.2 FRAM network

FRAM (F/(Ph)otometric Robotic Atmospheric Monitor) is a series of small robotic telescopes primarily designed for a continuous atmospheric monitoring of astronomical sites in order to measure atmospheric transparency with high spatial or temporal resolution. The original FRAM (Prouza et al. 2010) has been operated at the

Table 2. List of telescopes of the GRANDMA collaboration and their photometric performance when using their standard setup.

Telescope name	Location	Aperture (m)	FoV (deg)	Filters	Typical lim mag (AB mag)	Maximum night slot (UTC)
TAROT/TCH	La Silla Obs.	0.25	1.85 × 1.85	Clear, $g'r'i'$	18.0 in 60 s (Clear)	00–10 h
FRAM-Auger	Pierre Auger Obs.	0.30	1.0 × 1.0	BVR_CI_C, Clear	17.0 in 120 s (R_C)	00–10 h
CFHT/WIRCAM	CFH Obs.	3.6	0.35 × 0.35	JH	22.0 in 200 s (J)	10–16 h
CFHT/MEGACAM	CFH Obs.	3.6	1.0 × 1.0	$g'r'i'z'$	23.0 in 200 s (r')	10–16 h
Thai National Telescope	Thai National Obs.	2.40	0.13 × 0.13	Clear, $u'g'r'i'z'$	22.3 in 3 s (g')	11–23 h
Zadko	Gingin Obs.	1.00	0.17 × 0.12	Clear, $g'r'i'I_C$	20.5 in 40 s (Clear)	12–22 h
TNT	Xinglong Obs.	0.80	0.19 × 0.19	$BVg'r'i'$	19.0 in 300 s (R_C)	12–22 h
Xinglong-2.16	Xinglong Obs.	2.16	0.15 × 0.15	$BVRI$	21.0 in 100 s (R_C)	12–22 h
GMG-2.4	Lijiang Obs.	2.4	0.17 × 0.17	$BVRI$	22.0 in 100 s (R_C)	12–22 h
UBAI/NT-60	Maidanak Obs.	0.60	0.18 × 0.18	BVR_CI_C	18.0 in 180 s (R_C)	14–00 h
UBAI/ST-60	Maidanak Obs.	0.60	0.11 × 0.11	BVR_CI_C	18.0 in 180 s (R_C)	14–00 h
TAROT/TRE	La Reunion	0.18	4.2 × 4.2	Clear	16.0 in 60 s (Clear)	15–01 h
Les Makes/T60	La Reunion.	0.60	0.3 × 0.3	Clear, BVR_C	19.0 in 180 s (R_C)	15–01 h
Abastumani/T70	Abastumani Obs.	0.70	0.5 × 0.5	BVR_CI_C	18.2 in 60 s (R_C)	17–03 h
ShAO/T60	Shamakhy Obs.	0.60	0.28 × 0.28	BVR_CI_C	19.0 in 300 s (R_C)	17–03 h
Lisnyky/AZT-8	Kyiv Obs.	0.70	0.38 × 0.38	$UBVR_CI_C$	20.0 in 300 s(R_C)	17–03 h
TAROT/TCA	Calern Obs.	0.25	1.85 × 1.85	Clear, $g'r'i'$	18.0 in 60 s (Clear)	20–06 h
FRAM-CTA	ORM	0.25	0.43 × 0.43	Clear, BVR_Cz',	16.5 in 120 s (R_C)	20–06 h
IRIS	OHP	0.50	0.4 × 0.4	Clear, $u'g'r'i'z'$	18.5 in 60 s (r')	20–06 h
T120	OHP	1.20	0.3 × 0.3	$BVRI$	20.0 in 60 s (R)	20–06 h
OAJ/T80	Javalambre Obs.	0.80	1.4 × 1.4	r'	21.0 in 180 s (r')	20–06 h
OSN/T150	Sierra Nevada Obs.	1.50	0.30 × 0.22	BVR_CI_C	21.5 in 180 s (R_C)	20–06 h
CAHA/2.2m	Calar Alto Obs.	2.20	0.27⌀	$u'g'r'i'z'$	23.7 in 100 s (r')	20–06 h
VIRT	Etelman Obs.	0.50	0.27 × 0.27	$UBVRI$, *Clear*	19.0 in 120 s (Clear)	22–04 h

Table 3. List of telescopes of the GRANDMA collaboration with spectroscopic capabilities.

Telescope/Instrument	Location	Wavelength range	Spectral resolution λ/Δλ	Limiting mag
2.2-m CAHA/CAFOS	Calar Alto Obs.	3200–7000/6300–11000	400	20 in 1 h
ShAO/T2m	Shamakhy Obs.	3800–8000	2000	17 in 1 h
Xinglong-2.16/BFOSC	Xinglong Obs.	3600–9600	1000	18 in 1 h
GMG-2.4/YFOSC	Lijiang Obs.	3400–9100	2000	19 in 1 h
GTC	ORM	3630–7500/7330–10000	1018/2503	24 in 1 h

Pierre Auger Observatory in Argentina for more than a decade, while three more FRAMs (Janeček et al. 2019) are prepared to be used for a real-time atmospheric monitoring at Cherenkov Telescope Array (CTA) locations. Two of the FRAM sites are equipped, in addition to primary wide-field telephoto lenses, with larger diameter traditional telescopes, with larger diameter traditional telescopes intended for a follow-up and monitoring observations of a wide range of astrophysical transient objects (GRBs, variable stars, comets, etc). These two telescopes are used for GRANDMA network observations. The first is a 30 cm *f*/6.8 telescope located at Pierre Auger observatory, Malargue, Argentina, and equipped with *B*, *V*, *R*, and *I* filters, with an FoV of 60 arcmin × 60 arcmin and pixel scale of 0.92 arcsec pixel^{-1}. The second is a 25 cm *f*/6.3 telescope located at Observatorio del Roque de los Muchachos, La Palma, Canary Islands, Spain, and is equipped with *B*, *V*, *R*, and z' filters, with a 26 arcmin × 26 arcmin FoV and 1.52 arcsec pixel^{-1} pixel scale.

3.3 HETH group at IAA

The HETH (High-Energy Transients and their Hosts) group at the Instituto de Astrofísica de Andalucía (IAA) in Granada, Spain, continues to obtain competitive time at multiple telescopes. The programmes at the Observatorio de Sierra Nevada (OSN, PI: Blažek) and the Centro Astronómico Hispano en Andalucía (CAHA, PI: Kann) continue as detailed in Antier et al. (2020).

Competitive time was obtained at the Observatorio de Javalambre (OAJ) for further observations with the T80 telescope to obtain tiling observations (proposal number 1900160, PI: Kann, see Antier et al. 2020 for further details). Once again, the proposal was to observe 1.4° × 1.4° fields with an exposure time of 180 s each, reaching a typical limiting magnitude of $r' > 21.0$ mag. In this proposal, based on the lessons learned from O3a, the requested time was increased to 12.46 h (up to 100 tiles), including late-time re-observations for image-subtraction purposes. The second part of the proposal, multicolour KN follow-up, was dropped as GRANDMA has access to facilities that are better suited for such deep, narrow-field, targeted observations.

The Gran Telescopio Canarias[8] (GTC) is the world's largest single-aperture optical telescope, a 10.4-m Ritchey–Chrétien telescope with a segmented mirror located at 2267 m altitude at Roque de los Muchachos observatory, La Palma, Canary Islands, Spain, at 28°45′24″N, 17°53′31″W. It is equipped with a large suite of instruments. The following three are part of the proposal.

[8] http://www.gtc.iac.es

The Optical System for Imaging and low-Intermediate-Resolution Integrated Spectroscopy (OSIRIS) is a multipurpose imager and spectrograph mounted on the Nasmyth-B focus. It is equipped with SDSS $u'g'r'i'z'$ filters and multiple grisms and volume-phased holographic (VPH) gratings allowing for different spectral resolutions. We generally employ the R1000B (wavelength range 3630–7500 Å, resolution 1018 at 5455 Å) grism and the R2500I (wavelength range 7330–10000 Å, resolution 2503 at 8650 Å) VPH grating, as well as $g'r'i'z'$ imaging. To obtain spectra with sufficient S/N, exposures of different integration times are employed: 4×1200 s if the target has $r' > 22$ mag, 3×900 s for $r' \sim 20$–22 mag, and 2×900 s if $r' < 20$ mag.

The Especrografo Multiobjeto Infra-Rojo (Infrared Multi-Object Spectrograph, EMIR), installed at the Nasmyth-A focus, is a multichannel IR imager and medium-resolution spectrograph. For spectra, it can achieve an S/N of 7 for a 21 mag source with 4800 s of exposure in the $Y\,J$ grism. In imaging, limiting AB magnitudes at 5σ of $Y > 24.2$, $J > 23.6$, $H > 23.1$, and $K_S > 22.2$ mag can be achieved with exposure times of 180, 240, 420, and 600 s, respectively.

Finally, for the purpose of observing the host galaxy of a GW event in 3D, an application was made for time to use the Multi-Espectrógrafo en GTC de Alta Resolución para Astronomía (High-Resolution Multi-Spectrograph for Astronomy at GTC, MEGARA) in integral field unit (IFU) mode, covering a field of 12.5 arcsec × 11.3 arcsec with a spaxel size of 0.62 arcsec. Two grisms would be used to cover the spectral lines Hα, [N II], and [S II] as well as Hβ and [O III].

An award was made (proposal 118-MULTIPLE-3/20A, PI: Kann) 8 h of time with OSIRIS, 5 h with EMIR, and 2 h with MEGARA, ranked 'A'. The proposal was geared toward obtaining detailed observations of a single *confirmed* EM counterpart of a GW event, and not meant for classifying candidates. The observing time was valid for the last two months of O3, in 2020 March and April; however the worldwide COVID-19 pandemic caused GTC to be closed down already in mid-March, shortly thereafter followed by the end of O3b; no observations were ever triggered.

3.4 Thai National Telescope

The Thai National Telescope (TNT) located at Doi Inthanon National Park is the main facility for the National Astronomical Research Institute of Thailand (NARIT). It is s 2.4 m diameter, Ritchy–Chrétien telescope with an *f*/10 ratio, providing a plate scale of 8.6 arcsec mm^{-1} at the two Nasmyth foci. The telescope system is an alt-az mount that can slew at a speed of 4° s^{-1}; therefore, it can track or acquire optical transient sources rapidly with a pointing accuracy at less than 3 arcsec, and can track targets without autoguiding for 10 min or more with a pointing error of less than 0.5 arcsec. There are many scientific instruments that can be used upon request for specific observations such as ULTRASPEC (Dhillon et al. 2014) with SDSS filters ranging from 330 to 1000 nm, spectrographs varying from low to high resolution, and different types of scientific cameras.

The telescope was chosen to be built at the summit of the highest mountain in Thailand (Lat. 18.57372E°, Long. 98.48219E°, Alt. 2457 m). Its observational area and seeing conditions ensure dark skies for $B = 21.5$ and $V = 21.9$ mag arcsec^{-2}, and the median seeing is stable throughout the night at ≈0.9 arcsec.

3.5 VIRT

The Virgin Islands Robotic Telescope (VIRT) is the primary research telescope at the University of the Virgin Islands and is located at the Etelman Observatory on the island of St. Thomas in the US Virgin Islands. The facility is at an elevation of 381 meters, latitude of 18.3N and longitude of 64.9W. The VIRT is a 0.5-m Schmidt–Cassegrain telescope with a Finger Lakes Instrumentation (FLI) Proline 4240 back illuminated mid-band camera with an FLI Johnson/Bessel *UBVRI* filter set. Typical seeing at the site is 1.5−2.0 arcsec.

3.6 The *kilonova-catcher* citizen science program

Since the beginning of O3, GRANDMA has developed a citizen science program called *kilonova-catcher* (Antier et al. 2020). It allows non-professional astronomers to add their observational capabilities to the GRANDMA network in order to perform optical follow-up of GW candidates on a best-effort basis. During the O3b run, 33 *kilonova-catcher* users around the globe registered to the GRANDMA GW alert stream. In Fig. 7, we show the locations of the telescopes they could operate during the O3b run.

During the O3b campaign, the kilonova-cather program was active during the follow-up of two BNS merger candidates S191213g and S200213t. Because of the narrow FoV of the amateur telescopes, we coordinated their observations with a strategy based on targeted searches for optical transients located in promising host galaxies. From these two citizen observational campaigns, we obtained 57 follow-up images in total. A detailed description of the amateur observation strategy and results can be found in Section 5. GRANDMA is unique with this global initiative of citizen observers. O3 illustrated the huge potential for GW astronomy to vitalize sky observations and EM counterpart candidates, while also highlighting the need of training and coordinated joint analysis.

4 UPDATE FOR THE ALERT INFRASTRUCTURE, OBSERVATION STRATEGY AND WEB INTERFACE, AND DATA ANALYSIS USED IN GRANDMA

We use a similar infrastructure – *ICARE* (Interface and Communication for Addicts of the Rapid follow-up in multi-messenger Era) – for conducting coordinated observations of GW alerts to that discussed in Antier et al. (2020). ICARE relies on the automatic reception of a GW alert, creation of an automatic observation plan that is then sent to the telescopes of the network, a central database, and cloud applications to monitor the full network. Similar tools and infrastructure have been developed by other teams for a similar purpose, that is the GROWTH Marshal (Kasliwal et al. 2019). In this section, we will outline some improvements since the end of the O3a run, and in particular, during the break between O3a and O3b. We are going to focus on work done for the daily use version of ICARE that ran during O3b.[9] These modifications introduced some minor negative impacts on the productivity of the collaboration at the level of the end-user communication (i.e. mostly with regard to the preparation of GCNs), which had no effect on observations, nor results reported in this manuscript.

The PYTHON-based alert distribution system used by GRANDMA during O3a remained mainly the same. Upon receiving a GW candidate alerts through a GCN, the coverage of the sky localization region was generated for the GRANDMA collaboration telescopes (Table 2). For BBH-type events, only large FoV instruments were included, while all instruments were involved for NSBH or BNS type events if the posterior mean distance was below 300 Mpc. The resulting observation plans were then sent via VOEvent as soon as the

[9]There is a more 'universal version' of ICARE under development now that O3 has ended.

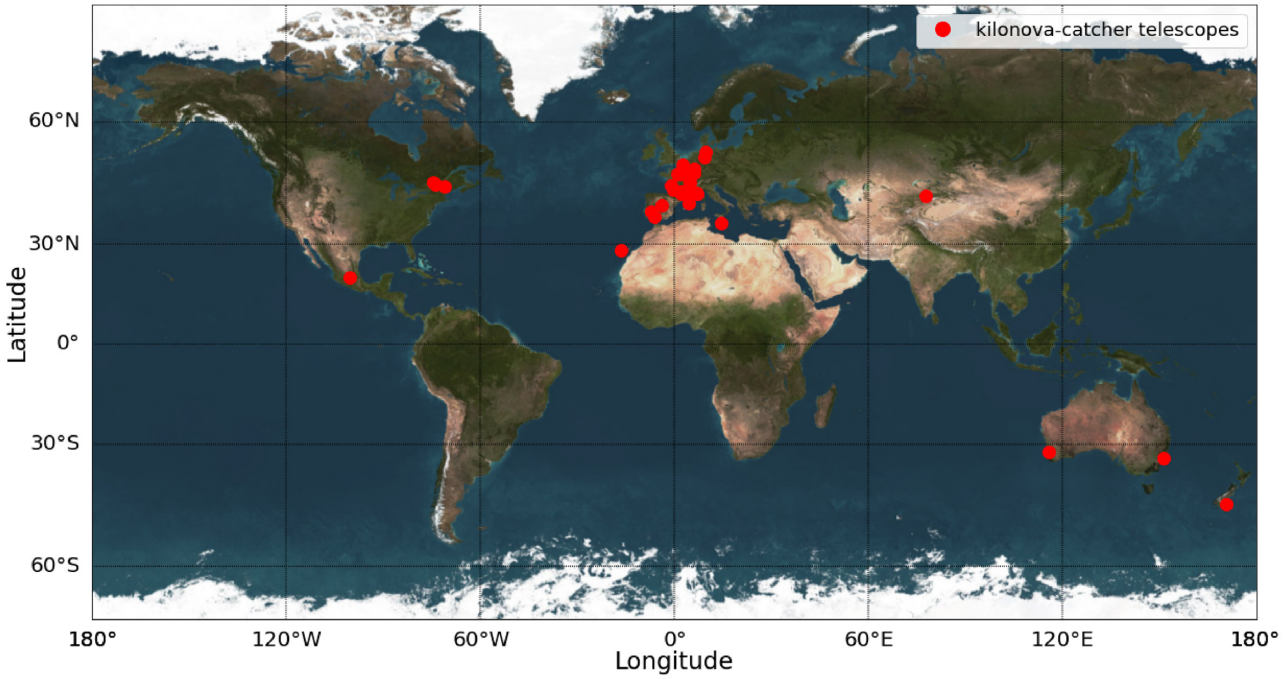

Figure 7. Locations of the 34 telescopes involved in the GRANDMA citizen science program: *kilonova-catcher*. Some citizen astronomers can operate several telescopes represented in this Earth map and also external remote facilities like the iTelescope Network (https://www.itelescope.net/), not represented here.

computation of a single plan was done using Comet.[10] We improved this system for O3b by introducing a forwarding of the retraction notice to avoid unnecessary observations.

Our observation plan algorithm benefitted from the continuous improvements of the GWEMOPT[11] telescope scheduling software (Coughlin et al. 2018a). Its latest version includes slicing sky localizations in right ascension to separately schedule different lobes in multilobed maps (Coughlin et al. 2019a), and automatically determining fields capable of being observed multiple times by several telescopes (Almualla et al. 2020). In doing so, the coverage of all our instruments, and especially the wide FoV telescopes, was improved. Our galaxy targeting strategy, that is when small FoV telescopes were utilized to survey known galaxies) was also revised using the dedicated MANGROVE galaxy catalogue presented in Ducoin et al. (2020a). We adopted the selection of preferential galaxies based on dependence on galaxy stellar mass. The most problematic issue in Galaxy Targeting Mode from O3a, however, that has since been addressed was the re-imaging of tiles when observations were executed. In short, this issue arose from an avoidance of considering whether or not a given galaxy requested for observation resided in the FoV of a preceding observation. As such, it resulted in an inefficient management of telescope observing time, and reduced the area covered by our collaboration. This improvement additionally benefited our strategy, as it led to extra time available for observing the most promising events.

The start of the O3 run demonstrated the need for a standard data reduction pipeline in order to homogenize the photometry within the network. First, we still use individual online image processing developed by the various groups such as TAROT and FRAM (Noysena et al. 2019). Secondly, we continue the development of a common detection pipeline *Gmadet*[12] adaptable for each telescope: it makes use of the popular AstrOmatic[13] software (SCAMP, SWARP, PSFEX, and SExTRACTOR) to perform the astrometric calibration, align and stack images, estimate the PSF and extract sources. The detected sources are crossmatched to different catalogues (Pan-STARRS, Gaia, USNO-B1) using Xmatch, the CDS crossmatch service, to discard already known objects. A crossmatch with known Solar system objects is also performed using SkyBoT (Berthier et al. 2006). Particular attention is paid to the photometric calibration so that magnitudes are expressed in the AB system. Image substraction with a reference image is performed using HOTPANTS (Becker 2015), where Pan-STARRS stacked images can be used as reference. A Convolutional Neural Network algorithm is trained to identify stellar sources and discard most of the cosmics, bad pixels or artefacts coming from the subtraction process. In practice, during O3b *Gmadet* was used to detect transient candidates in parallel to individual standard online image processing made by the groups. The results presented in this work correspond for *Gmadet* only for the OAJ observations of S200213t. The other results use the individual image processing described in Antier et al. (2020) to allow for a direct comparison of our results against those for O3a. In case of GW alert observations engaged by GRANDMA, each individual image was processed with a search for point sources detected at the 5-or greater level. All the false positives which were deemed to be artieacts or cosmic rays, were eliminated by human inspection.

[10]https://comet.transientskp.org/en/stable/
[11]https://github.com/mcoughlin/gwemopt
[12]https://github.com/dcorre/gmadet
[13]https://www.astromatic.net

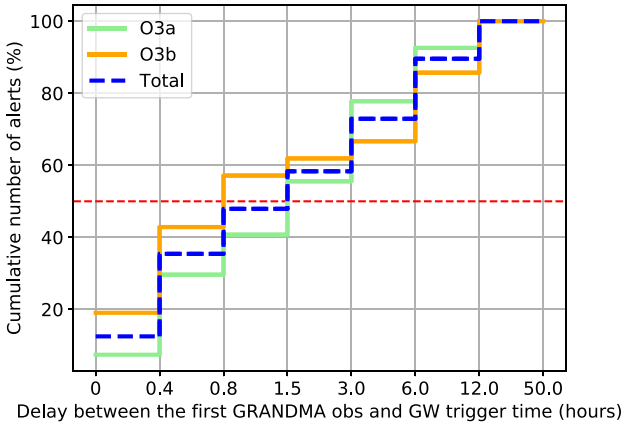

Figure 8. Cumulative distribution of the delay between the GW candidate/event trigger time and the first observation done by GRANDMA. The minimal delay is about 15 min obtained with both the TAROT and FRAM networks. About 50 per cent of the sky localization areas of GW candidate/event alerts have been observed with a minimal delay of 1.5 h.

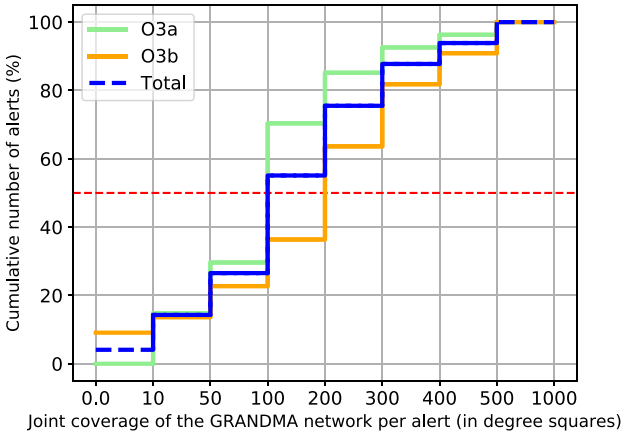

Figure 9. Cumulative distribution of the total sky coverage of the GRANDMA network (in deg^2) engaged for each GW candidate/event alert. The distribution depends on the sky localization area size of the alerts and observability constraints, as discussed in Section 2.

5 GRANDMA ELECTROMAGNETIC FOLLOW-UP CAMPAIGN OF O3A AND O3B

5.1 Observational summary of GRANDMA for O3a and O3b

Over the 11 months of observations of the O3 campaign, GRANDMA followed-up 49/56 candidate events: 27/33 for O3a and 22/23 for O3b. The observation efficiency for GRANDMA is therefore ∼82 per cent for O3a and 96 per cent for O3b. This high cadence is possible due to the organization of the GRANDMA collaboration and the automated infrastructure discussed above. It is significantly above the reported observational rate of other ground-follow-up teams, aside from MASTER-Net (Lipunov et al. 2010) that reports GCNs for every alert based on their automated observations. Based on the GCN traffic, GRANDMA can be compared to GROWTH (about 30 per cent of alerts, Coughlin et al. 2019c), GOTO (about 15 per cent of alerts, O'Brien 2018), ENGRAVE (about 5 per cent of alerts, Ackley et al. 2020), GRAWITA (about 25 per cent of alerts, Salmaso et al. 2019), J-GEM (about 7 per cent of alerts, Kaneko & J-GEM Collaboration 2020), NOWT (about 4 per cent of alerts, Zhu et al. 2019), SAGUARO (about 11 per cent of alerts, Lundquist et al. 2019), and SVOM (about 30 per cent of alerts, Xin, SVOM Multi Messenger Astronomy Team & GWAC Team 2020).

As shown in Fig. 8, GRANDMA performed its first observation at most 1.5 h after the GW trigger time for more than half of the alerts, and at most 30 min for 15 per cent of the alerts during O3. The minimal delay between the GW trigger time and the first GRANDMA observation is 15 min, which includes the ∼5 min delay for sending the alert by LIGO/Virgo, ∼5 min for computing the observation plan, and ∼5 min for scheduling by the telescope. This has been achieved for both the TAROT and FRAM networks. Moreover, we see some improvement in terms of the rapid response by GRANDMA between O3a and O3b: this is due to improvements not only from the LIGO/Virgo infrastructure system (Abbott et al. 2019a) but also the GRANDMA infrastructure improvements discussed above. This demonstrates once more the need for a heterogenous network of telescopes sharing joint tools to face the challenge of follow-up of GW triggers and their requirement of rapid EM observational responses. Indeed, Metzger (2019) and references therein, predict different light-curve evolutions for the first hours after the merger of two compact objects (Arcavi 2018) depending on the properties of the initial binary system. Early time observations after the merger (less than two hours and in different passbands if possible) might have provided important constraints on properties of the fast ejecta components, the composition of the ejected material, and the heating rate for the unbound material. Other contribution channels or kilonova-precursors powered by free neutron decay can also be ruled out by early observations (Metzger et al. 2015).

GRANDMA covered 213 ± 173 deg^2 on average for the GW alerts during O3. As shown in Fig. 9, more than 100 deg^2 of the sky has been observed by the GRANDMA network for more than half of the alerts. We do not see major differences in terms of sky coverage between O3a and O3b; however, improvements in the network-level scheduling as discussed in Coughlin et al. (2019a) in 2019 June led to a significant increase of the maximum coverage reachable by GRANDMA (typically by a factor of 2). The total maximal coverage for a single alert was for S191204r, a BBH candidate event, at 550 deg^2, representing 90 per cent of the sky localization area. The lowest coverage was only 10 per cent of the candidate S200225q's most updated sky localization area; although the event was well localized, with a 90 per cent credible region of 22 deg^2 as seen in Appendix A and LIGO Scientific Collaboration & Virgo Collaboration (2020k), the vast majority of this region was behind the sun at the time of the event. In Fig. 10, we can see the total sky coverage of GRANDMA over the full O3 campaign. There is a clear distribution of Northern and Southern hemispheres among the different telescopes due to the global coordination (see Section 4). In total, we covered 9218 deg^2 with six wide FoV telescopes, with multi-epoch observations for most of the fields. Our near real-time analysis did not find any interesting kilonova candidates (see Section 5 and Antier et al. 2020).

According to Fig. 2, the median distance of O3 BNS merger candidates is ∼200 Mpc, corresponding to a distance modulus, DM = 36.5. The median distance of BBHs is ∼1.3 Gpc (DM = 40.6). Considering an apparent limiting magnitude of 17, this corresponds to approximate absolute magnitude non-detection limits of −19.5 for BNSs and −23.6 for BBHs. Fig. 11 displays the absolute magnitude limit based on the distance of each GW event versus the observed area, and in Fig. 12, versus the time of the first optical observations. It shows that only 12 GW events were observed by GRANDMA covering more than 80 per cent of the error box. The names of these events are indicated in the Fig. 11. Essentially only BBH events have

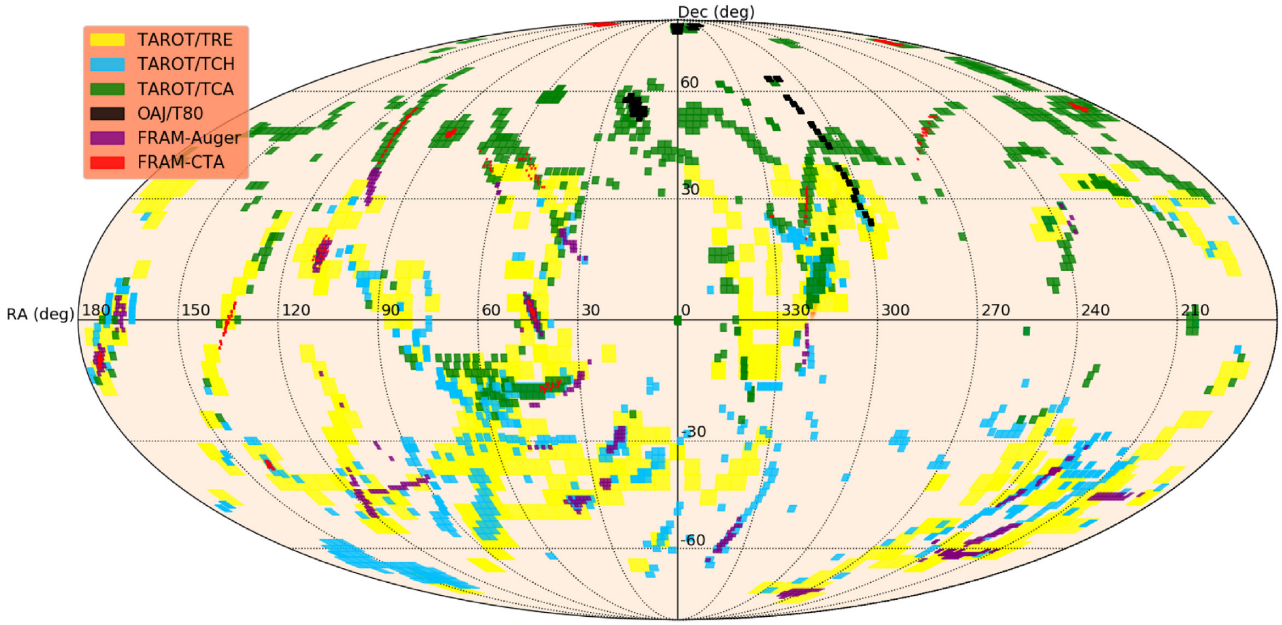

Figure 10. Total sky coverage of the wide FoV telescopes of GRANDMA during O3. Note the distribution of observations due to the GRANDMA coordinated program. Also note that the heterogeneity of the maps is imprinted from observing constraints and the distribution of the alerts over the sky.

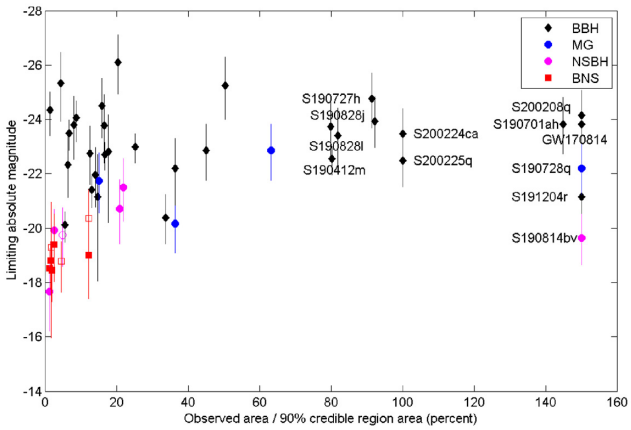

Figure 11. All LIGO/Virgo GW candidates/events observed by GRANDMA telescopes are plotted as limiting absolute magnitude versus the percentage of the 90 per cent credible region that was observed. We added the TAROT/TRE limit of GW 170814 published in Noysena et al. (2019). candidates/events having a percentage of the 90 per cent credible region greater than 150 per cent are plotted at 150 per cent to keep clarity of the plot.

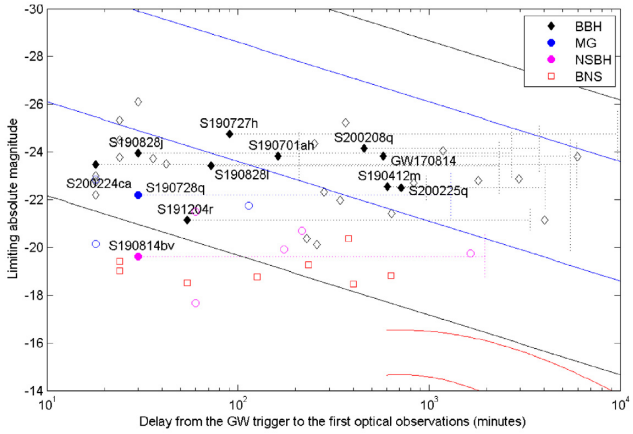

Figure 12. All LIGO/Virgo GW candidates/events observed by GRANDMA telescopes are plotted as limiting absolute magnitude versus the delay between the GW trigger and the first GRANDMA observations. Filled symbols are used for candidates/events for which more than 80 per cent of the 90 per cent credible region have been observed. We added the TAROT/TRE limit of GW170814 published in Noysena et al. (2019). The dashed horizontal bars indicate the duration of the first visit for the best candidates/events (selected from the Fig. 11). The black lines are the typical limits of LGRB light curves, blue lines for SGRBs, and red lines for the GW170817 kilonova.

full coverage of the credible region; this is due to a combination of the statistical rate of observability (see Section 2.2), GRANDMA coverage capacity (∼200 deg^2), and the poor localization of NSBH or BNS events. S190814bv, with a current classification of NSBH, remains the exception. In conclusion, the disparity of alerts during O3 in terms of localization and their observational accessibility, the evolution of the localization over time, as well as the possible nature of candidates, shows a clear need for monitoring of routine observations of the alerts and calls for rapid reactions at all times. In this way, by observing all alerts during O3, GRANDMA has gained training and experience and is ready to observe a large number of alerts during the subsequent GW observation campaigns, starting with O4.

5.2 Report summary of GRANDMA observations during O3b

Specifically for O3b, we report our observations for the BBH candidates in Table 4, and for the systems potentially containing at least one NS in Table 5. The unmodelled GW burst candidate S200114f is listed in Table 6. All the sky localization coverage are shown in Appendix A.

We have similar observational results during O3b as in O3a in terms of coverage; at least 30 per cent of the error boxes of the GW candidate events (using the most recently updated sky localization

Table 4. Summary of the GRANDMA observations during the last five months of O3 for BBH candidates. Observations are not necessarily continuous during the time interval. S191110x S191213ai, S191120at, S191124be, S191212q, S191225aq, S200108v, and S200303ba, were retracted by the LVC due to data quality issues in the detectors.

Alert	Time (UTC)	Type	Dist (Mpc)	90 per cent c.r. (deg^2)	Telescope	δt (h)	ΔT (h)	Lim. mag	Prob (per cent)	Area (deg^2)
S191105e	14:35:21	BBH (95 per cent)	1183 ± 281	643	GRANDMA	49.0	16.2	17–18	64.1	289
					FRAM-Auger	57.6	1.6	16.8	3.6	19
					FRAM-CTA	58.7	1.5	15.9	0.2	4
					TCA	56.1	6.4	18	1.1	25
					TCH	57.4	7.9	18	33.6	46
					TRE	49.0	8.47	17	57.3	242
S191109d[a]	01:07:17	BBH (>99 per cent)	1810 ± 604	1487	GRANDMA	0.4	31.2	17–18	18.0	263
					FRAM-Auger	5.7	1.8	16.0	2.8	19
					FRAM-CTA	0.4	2.7	16.0	0.5	5
					TCA	1.0	26.0	18	2.1	43
					TCH	29.5	2.2	18	1.0	11
					TRE	20.2	2.5	17	12.3	191
S191129u	13:40:29	BBH (100 per cent)	742 ± 180	852	GRANDMA	10.6	49.1	18	27.9	130
					FRAM-Auger	11.3	2.2	16.2	6.1	17
					TCA	10.6	5.5	18	4.6	63
					TCH	10.7	49.0	18	21.9	63
S191204r[a]	17:15:26	BBH (100 per cent)	678 ± 149	103	GRANDMA	0.9	58.6	18	89.1	550
					FRAM-Auger	7.4	1.7	16.7	0.1	20
					TCA	0.9	57.1	18	0.8	68
					TCH	7.5	30.4	18	18.2	68
					TRE	1.0	47.8	17	72.9	417
S191215w	22:30:52	BBH (>99 per cent)	1770 ± 455	361	GRANDMA	0.6	56.3	17–18	37.3	288
					FRAM-Auger	5.0	1.4	16.7	2.1	20
					FRAM-CTA	46.1	0.2	17.5	0.7	1
					TCA	42.6	5.1	18	18.6	25
					TCH	2.2	54.7	18	13.0	36
					TRE	0.6	47.3	17	8.6	226
S191216ap	21:33:38	BBH (99 per cent)	376 ± 70	253	GRANDMA	3.8	162.1	17–18	42.8	85
					FRAM-Auger	3.8	1.1	15.1	1.8	8
					FRAM-CTA	21.6	1.5	17.4	4.4	5
					TCA	19.4	146.4	18	40.1	67
					TCH	27.6	122	18	0.7	11
S191222n	03:35:37	BBH (>99 per cent)	2518 ± 679	1850	GRANDMA	0.4	51	17–18	23.8	292
					FRAM-Auger	0.4	28.4	16.3	3.0	20
					FRAM-CTA	0.7	1.5	16.6	0.3	5
					TCA	0.7	1.2	18	3.6	71
					TCH	3.0	48.5	18	8.8	56
					TRE	12.5	30.5	17	10.0	157
S200112r	15:58:38	BBH (>99 per cent)	1125 ± 289	4004	GRANDMA	0.3	58.8	17–18	16.9	500
					FRAM-Auger	9.5	5.2	15.4	0.5	15
					FRAM-CTA	13.5	25.6	16.6	0.7	5
					TCA	1.5	48.8	18	5.8	71
					TCH	8.6	50.5	18	2.4	63
					TRE	0.3	47.9	17	8.7	379
S200115j	04:23:09	MassGap (>99 per cent)	340 ± 79	765	GRANDMA	0.3	166.3	17–18	14.8	278
					FRAM-Auger	20.8	1.7	15.8	1.6	19
					FRAM-CTA	15.3	1.5	17.4	0.4	5
					TCA	12.9	153.8	18	3.8	71
					TCH	0.3	164.9	18	6.5	68
					TRE	11.7	28.8	17	7.4	174

Table 4 – *continued*

Alert	Time (UTC)	Type	Dist (Mpc)	90 per cent c.r. (deg^2)	Telescope	δt (h)	ΔT (h)	Lim. mag	Prob (per cent)	Area (deg^2)
S200128d	02:20:11	BBH (97 per cent)	3702 ± 1265	2293	GRANDMA	0.4	54.7	17–18	11.2	97
					FRAM-Auger	0.45	5.6	17.8	2.6	20
					FRAM-CTA	0.4	4.8	16.8	0.4	4
					TCA	19.1	3.2	18	1.5	22
					TCH	2.6	52.5	18	8.7	67
S200129m	06:54:58	BBH (100 per cent)	755 ± 194	41	GRANDMA	11.0	12.2	18	8.3	7
					TCA	11.0	12.2	18	8.3	7
S200208q	13:01:17	BBH (>99 per cent)	2142 ± 459	26	GRANDMA	7.6	104.0	17–18	95.1	488
					FRAM-Auger	18.3	0.12	16	8.6	2
					FRAM-CTA	9.3	0.98	15.3	11.3	3
					TCA	7.6	104.0	18	0.1	69
					TCH	11.4	56.5	18	43.6	69
					TRE	27.0	8.9	17	91.1	364
S200219ac	09:44:15	BBH (96 per cent)	3533 ± 1031	781	GRANDMA	6.1	53.1	17–18	39.2	392
					FRAM-Auger	14.7	1.6	16.5	4.8	17
					FRAM-CTA	13.3	1.5	17.3	0.8	4
					TCA	8.5	50.7	18	8.6	70
					TCH	14.6	27.6	18	11.2	63
					TRE	6.1	31.9	17	23.8	277
S200224ca	22:22:34	BBH (>99 per cent)	1575 ± 322	72	GRANDMA	0.3	99.3	17–18	92.5	169
					FRAM-Auger	6.9	1.8	16.9	51.9	18
					FRAM-CTA	0.3	1.5	16.5	19.2	4.0
					TCA	0.3	99.3	18	1.4	26
					TCH	5.0	52.9	18	20.9	32
					TRE	0.8	98.2	17	90.6	139
S200225q	06:04:21	BBH (96 per cent)	995 ± 188	22	GRANDMA	12.0	58.2	17–18	10.2	277
					FRAM-Auger	18.1	3.8	16.4	0.1	20
					FRAM-CTA	13.8	28.7	17.2	9.7	9
					TCA	12.0	58.1	18	0.4	81
					TCH	18.4	51.8	18	<0.1	74.0
					TRE	11.9	26.7	17	<0.1	106
S200302c	01:58:11	BBH (89 per cent)	1820 ± 536	5656	GRANDMA	1.0	71.5	17–18	18.0	450
					FRAM-Auger	1.0	1.9	16.1	1.6	19
					TCA	17.5	54.9	18	6.3	92
					TRE	17.0	28.7	17	10.9	349
S200311bg	11:58:53	BBH (100 per cent)	1115 ± 175	34	No observations, Sun-constrained					
S200316bj	21:57:26	MassGap (>99 per cent)	1178 ± 283	508	GRANDMA	0.3	119.9	17–18	73.3	321
					FRAM-Auger	1.8	1.6	16.1	1.3	16
					FRAM-CTA	0.4	1.4	17.1	15.0	4
					TCA	0.3	52.5	18	68.0	69
					TRE	41.7	6.4	17	4.9	244

Notes: 90 per cent c.r. corresponds to the 90 per cent credible region of the latest sky localization area sent by LIGO-Virgo ([a], when only the 'Bayestar sky localization' is available), δt to the delay with respect to the trigger time, ΔT to the duration of the observations, Prob (per cent), and Area (deg2) to the coverage of GRANDMA compared to the latest revision of the sky localization area in percentage and in squares degrees. Limiting magnitudes are computed from 5σ threshold for source extraction.

areas) were observed in 63 per cent of the cases. The TAROT network followed and reported search results (Noysena et al. 2019) for all of the GW alerts sent by GRANDMA, and FRAM only missed one of them. We note also the participation of the OAJ telescope for the BNS candidate S200213t (LIGO Scientific Collaboration & Virgo Collaboration 2020h; Blazek et al. 2020a). The participation of the narrow FoV telescopes has been reduced in O3b to host galaxy targeting searches due to a low number of GW candidates with a most probable luminosity distance below 300 Mpc; this consisted of three events (LIGO Scientific Collaboration & Virgo

Table 5. Summary of the GRANDMA observations during the last five months for BNS or NS–BH merger candidates, using the latest versions of the LALInference sky localizations ([a], when only the 'Bayestar sky localization' is available). Observations are not necessarily continuous during the time interval. S191117j, S191120aj, S191213ai, S191220af, S200106au, S200116ah, and S200308e, were retracted by the LIGO-Virgo collaboration due to data quality issues in the detectors.

Alert	Time (UTC)	Type	Dist (Mpc)	90 per cent c.r. (deg^2)	Telescope	δt (h)	ΔT (h)	Lim. mag	Prob (per cent)	Area (deg^2)
S191205ah[a]	21:52:08	NSBH (93 per cent)	385 ± 164	6378	GRANDMA	2.9	151.6	18	4.8	158
					FRAM-Auger	8.2	1.4	16.5	0.5	20
					TCA	18.9	133.2	18	3.0	71
					TCH	2.9	151.6	18	1.2	68
S191213g	04:34:08	BNS (77 per cent)	201 ± 81	4480	GRANDMA	0.9	120.4	18	0.6	43
					FRAM-CTA	0.9	0.3	15.2	<0.1	1
					TCA	47.6	73.3	18	0.5	42
					Kilonova-catcher	39.8	13	18	<1	<1
S200105ae	16:24:26	NSBH (3 per cent)	282 ± 74	7373	GRANDMA	27.5	130.2	17–18	12.5	356
					FRAM-Auger	60.0	1.7	15.8	0.6	20
					FRAM-CTA	28.1	1.5	16.3	0.2	5
					TCA	27.5	118.2	18	3.2	70
					TCH	59.0	98.7	18	3.3	70
					TRE	48.0	26.5	17	9.9	295
S200213t	04:10:40	BNS (63 per cent)	201 ± 80	2326	GRANDMA	0.4	164.8	16–21	32.8	281
					FRAM-Auger	20.3	1.3	16.0	0.1	15
					FRAM-CTA	15.3	1.5	17.3	4.0	4
					TCA	0.4	163.3	18	30.4	70
					TCH	45.1	120.1	18	<0.1	4
					TRE	12.0	31.0	17	0.8	193
					OAJ	15.0	1.5	20.1	17.5	25
					UBAI/NT-60	161.8	73.9	17	<1	<1
					UBAI/ST-60	161.0	73.1	17	<1	<1
					VIRT	187.3	0.5	17	<1	<1
					Kilonova-catcher	22.0	120	16–19	<1	<1

Notes: 90 per cent c.r. corresponds to the 90 per cent credible region of the latest sky localization area sent by LIGO-Virgo, δt to the delay with respect to the trigger time, ΔT to the duration of the observations, Prob (per cent), and Area (deg^2) to the coverage of GRANDMA compared to the latest revision of the sky localization area in percentage and in squares degrees. Limiting magnitudes are computed from 5σ threshold for source extraction.

Table 6. Summary of the GRANDMA observations of the S200114f unmodelled ('burst') GW candidate detected on 2020 January 14 at 02:08:18 UT.

Telescope	δt (h)	ΔT (h)	Lim. mag	Prob (per cent)	Area (deg^2)
GRANDMA	0.3	90.7	17–18	76.4	351
FRAM-Auger	0.3	1.7	16.2	28.5	19
FRAM-CTA	0.3	1.7	16.2	7.4	5
TCA	15.6	76.1	18	13.4	11.2
TCH	15.1	35.6	18	14.0	39
TRE	15.0	31.4	17	68.2	311

Notes: The 90 per cent credible region of the event spans 403 deg^2. An addition burst candidate S191110af was retracted by the LVC due to a data quality issue in the detectors. δt corresponds to the delay with respect to the trigger time, ΔT to the duration of the observations, Prob (per cent), and Area (deg^2) to the coverage of GRANDMA compared to the sky localization area in percentage and in squares degrees. Limiting magnitudes are computed from 5σ threshold for source extraction.

Collaboration 2020h, 2019o, a). However, we can highlight the participation of the Lisnyky and Tingshua groups for S191213g, the UBAI group for S191213t, and the VIRT group for S200213t. We also highlight the participation of amateur astronomers for S191213g and S200213t.

5.3 The binary neutron star merger candidate S191213g

The GW candidate S191213g was detected on 2019 December 13 04:34:08 UTC (LIGO Scientific Collaboration & Virgo Collaboration 2019o). The trigger was identified by Virgo, LIGO-Hanford, and LIGO-Livingston with a reported false alarm rate of 1.12 yr^{-1}. It has a non-negligible probability of 23 per cent of being of terrestrial origin, but assuming its origin is astrophysical, the GWs were likely emitted from a BNS (BNS 77 per cent). Using the low-latency analysis (Kapadia et al. 2020), if it is astrophysical, it has more than 99 per cent chance to have a remnant. The low-latency localization analysis (Singer & Price 2016) gave an estimated distance of 195 ± 59 Mpc, and a 90 per cent credible sky area localization of 1393 deg^2 (LIGO Scientific Collaboration & Virgo Collaboration 2019o). The next day, the offline analysis performed by LALInference (Veitch et al. 2015) gave a distance of 201 ± 81 Mpc and a poorer localization with a 90 per cent sky area of 4480 deg^2 (LIGO Scientific Collaboration & Virgo Collaboration 2019q). As S191213g is considered a potential BNS event, several teams performed follow-up in both neutrino and EM domains. Concerning neutrinos, no candidates were found by IceCube (IceCube Collaboration 2019), ANTARES (Ageron et al. 2019), or the Pierre Auger Observatory (Alvarez-Muniz et al. 2019). Concerning photons, at high energies, *INTEGRAL* (Gotz et al. 2019), *MAXI* (Sugita et al. 2019), *AGILE* (Verrecchia et al. 2019; Casentini et al. 2019), *Fermi*/GBM and LAT (Wilson-Hodge,

Fermi-GBM Team & GBM-LIGO/Virgo Group 2019; Cutini et al. 2019), *Swift* (Barthelmy et al. 2019), *CALET* (Marrocchesi et al. 2019), *AstroSat* (Shenoy et al. 2019), and *Insight*-HXMT(Xiao et al. 2019) did not detect any transients in the 90 per cent credible region. In the optical, Zwicky Transient Facility (ZTF) published two lists of 9 and 10 candidates, respectively (Andreoni et al. 2019; Stein et al. 2019). All of them were ruled out after spectroscopic vetting or looking at archival data from wide FoV telescopes.

5.3.1 GRANDMA follow-up of the GW alert for S191213g

Observation plans were sent to 17 GRANDMA telescopes as the event distance enables the search for counterparts located close to interesting galaxies. Unfortunately, the time of the event was relatively close to the end of the European night, and combined with the minimal coverage possible, mostly constrained to the Northern hemisphere; rapid observations by GRANDMA were not an easy task. Due to the low significance of the event, we preferred not to engage our Target of Opportunity (ToO) time and instead concentrated our effort on following up some possible EM candidates reported by others. Two of our robotic telescopes performed observations to follow up the event: FRAM-CTA-N and TCA. FRAM-CTA-N started observations 53 min after the GW trigger in the R_c band and TCA started 2858 min after the GW trigger with no filter. These observations covered about 3.4 per cent of the cumulative probability of the Bayestar sky localization area created at 2019 December 13 04:36:53 (UTC), representing only 1 per cent of the most recently updated LALInference localization (LIGO Scientific Collaboration & Virgo Collaboration 2019r). No significant transient candidate was found during our real time analysis. We also note that none of the candidates found by other teams were contained in fields observed by FRAM or TCA.

We also conducted follow-up observations via the citizen-scientist programme. As soon as the alert was received, we ranked the 200 most promising host galaxies spatially compatible with the GW skymap following the method described in Ducoin et al. (2020a). This list was promptly distributed to the *kilonova-catcher* community to perform targeted searches for optical transients. The citizen-astronomers were asked to favour the best-ranked galaxies for their observations and to use a clear filter in order to maximize the chances of detection. The idea was to maximize their discovery potential before performing multiband follow-up observations to confirm an optical transient candidate and study its physical properties. From this citizen observational campaign, we obtained 13 follow-up images, with 16 galaxies localized in the 90 per cent C.L. probability sky area. The amateur observations started between 1.87–2.2 d after the GW trigger. All the observations are reported in Appendix Table B1. No optical transient was found at any galaxy position and constraints on their underlying optical flux were derived, resulting in typical unfiltered limiting magnitude of $m_{\rm Lum} = 17.6 \pm 0.2$ at 5σ confidence.

5.3.2 GRANDMA follow-up of the electromagnetic counterpart candidate AT2019wxt

At 2019 December 18, Pan-STARRS published a GCN about a potential counterpart, AT2019wxt/PS19hgw (now named SN 2019wxt), located in the galaxy KUG 0152+311 at a distance of 144 Mpc, and compatible with the GW localization (McBrien et al. 2019). Its place in the localization area and its blue and quite featureless spectrum made SN 2019wxt an interesting kilonova candidate. Eventually, the transient was ruled out by the VLT (Vogl et al. 2019) due to the discovery of broad helium emission lines which are usually found in Type Ib supernovae (SNe); such a blue continuum had already been observed in the early phases of Type IIb SNe. The final classification of AT2019wxt as a Type IIb SN was done by LBT (Vallely et al. 2019).

On the GRANDMA side, Lisnyky/AZT-8 observed the transient location on 2019 December 18 between 20:39:20 and 21:19:07 (UTC). Stacking the 40 images, the OT was not detected up to an upper limit of 19.0 mag in the R_C band.

The Tingshua-NAOC Telescope (TNT, Wang et al. 2008; Huang et al. 2012) was also observing on 2019 December 18 between 16:53:05 and 17:03:05 (UTC) in the g' band, on 2019 December 19 in the $BVg'r'i'$ bands, and on 2019 December 26 in the $g'r'i'$ bands. The source was barely visible because of bad seeing. The upper limit results are reported in the Vega system for the BV bands and in the AB system for the $g'r'i'$ bands in Appendix C1.

The 2.16-m telescope located in Xinglong observed on 2019 December 27. The source was very faint in the V band, making the measurements inaccurate, whereas it was readily visible in the R band. The techniques in photometry employed for both TNT and Xinglong/2.16 m were image subtraction, with templates that were created by interpolating from the surrounding pixels using the Laplace method.

The TNT, equipped with ULTRASPEC, the high-speed camera, obtained images in $u'g'r'i'z'$ on 2019 December 20 UTC. After a month it revisited the position again, on 2020 January 16 UTC. The transient magnitude was measured by subtracting the galaxy background using the image of the galaxy obtained after the transient had faded, before doing photometry, with PSF fitting. We obtained detections with $u' = 20.72 \pm 0.29$ mag, $g' = 19.60 \pm 0.18$ mag, $r' = 19.58 \pm 0.30$ mag, $i' = 19.34 \pm 0.23$ mag, and $z' = 19.30 \pm 0.35$ mag, with a median S/N and limiting magnitude of 4.0 and 20.0 mag, respectively.

The citizen astronomers performed observations, and the results are presented in Appendix Table C1. Three astronomers, M. Serrau, D. St-Gelais, and H.-B. Eggenstein sent images of the transient location. The data reduction was done by using references images taken by the same astronomers to perform host subtraction, and the photometric calibration was done using the Pan-STARRS catalogue. For M. Serrau and H.-B. Eggenstein, the transient was not visible to a limiting magnitude of 17.7 in the luminance filter and 18.10 in the I_C band. In D. St-Gelais' image, the transient is visible with a magnitude of 18.8 in the luminance filter. As this is a point source with a well-known position, all limits are given at 3σ confidence.

A light curve of SN2019wxt with photometric points reported in GCNs and with the GRANDMA measurements can be seen in Fig. C1. We conducted an independent investigation for determining the possible nature of the AT2019wxt using the photometric evolution of the light curve in the g and r bands. We use the method proposed in Stachie et al. (2020b); it relies on a deep-learning algorithm (Muthukrishna et al. 2019), which was previously trained on ZTF-like transient light curves (see a more extended description of the training data set in these references). Each data were classified in different categories: 'SN' (supernovae such as SNIa, SNIb, SNIc, SNII), 'KN' (kilonova) and 'Others' (regrouping various types of transients such as active galactic nuclei, AGNs, tidal disruption events). The algorithm also reports as 'Indistinguishable' cases when either there is not enough data (few observations) or the classifier does not recognize the light curve. As demonstrated in Stachie et al. (2020b), the algorithm is efficient for classify a wide variety of publicly reported ZTF SNe during the testing sequence. By extension, the simulated kilonovae that can be observed by ZTF

are well classified by this procedure, with an efficiency higher than 50 per cent after around 10 observations. In the case of AT2019wxt, the situation is more complex due to a heterogeneous data set made by various observatories different than ZTF (whereas training was only done with ZTF), with different photometric measurement techniques, irregular time of observations, and the lack of further measurements after 20 d. However, about 20 data points in g and r bands (see in Appendix C1) have been used; the algorithm classified the transient as 'Indistinguishable' after each new observation, and does not favour a kilonova classification. Given the extensive observations, the non-identification of the transient likely indicates that AT2019wxt is a peculiar transient.

We also compare this light curve to expected kilonovae models. To do so, we employ a Gaussian process regression-based surrogate model (Doctor et al. 2017; Coughlin et al. 2018b, 2019b, 2020a) that employs pre-computed kilonova light curves modelled with the full radiative-transfer Monte Carlo code of Kasen et al. (2017). This allows us to compute arbitrary light curves for generic ejecta properties/configurations. This analysis finds that at the distance of the host galaxy, the ejecta masses required approach 0.1 $M_\odot$ and beyond, higher than expected in BNS mergers. In addition, even a two-component model, for the parameter space considered, is unable to reproduce the u- and g-band excesses seen in this particular transient, although the evolution in the redder bands is broadly consistent. In this way, a kilonova explanation for this transient is disfavoured within the expected parameter space for these types of transients.

The rapidly declining light curves of SN 2019wxt suggest a possibility that this SN could be powered by the interaction of the ejecta with circumstellar materials (CSM; e.g. Chatzopoulos, Wheeler & Vinko 2012; Chatzopoulos et al. 2013; Wang et al. 2019). Assuming that the CSM has a stellar-wind density profile (i.e. $\rho \propto r^{-2}$) and that the density is uniform for the inner ejecta and follows $\rho \propto r^{-7}$ for the outer ejecta, a fit to the multiband data (corrected for galactic extinction) of this SN is obtained with χ^2/d.o.f. = 43. The corresponding parameters include $T_0 = 58830.190$, $M_{\rm ej} = 0.87\,M_\odot$, $v_{\rm ej} = 9.33 \times 10^8$ cm s^{-1}, $M_{\rm CSM} = 0.16\,M_\odot$, $\rho_{\rm CSM,\,in} = 8.25 \times 10^{-12}$ g cm^{-3}, $r_{\rm CSM,\,in} = 1.8 \times 10^{14}$ cm, and $\epsilon = 0.1$, where T_0 is the explosion date, $M_{\rm ej}$ is the mass of ejecta, $v_{\rm ej}$ is the velocity of ejecta, $M_{\rm CSM}$ is the mass of CSM, $\rho_{\rm CSM,\,in}$ is the density at the inner radius of the CSM ($r_{\rm CSM,\,in}$), and ϵ is the radiation efficiency. As seen in Fig. 13, we compare the fit to the results with the evolution in different colours, which could minimize the effect of the difference in observed brightnesses from different telescopes. If the CSM results from a mass ejection of the progenitor star before explosion, the mass-loss rate can be estimated as $0.05/(v_{\rm CSM}/10$ km s$^{-1})$ $M_\odot$ yr^{-1}, where $v_{\rm CSM}$ is the velocity of the CSM. Wolf–Rayet stars or red supergiant stars have difficulty in producing such intense ejections; while binary interaction can possibly be responsible for mass ejection of 10^{-3}–$10^{-1}\,M_\odot$ yr^{-1} (see Smith 2014; Bhirombhakdi et al. 2019, and references therein). Therefore, SN 2019wxt could possibly originate from an explosion of a binary star.

5.4 The unmodelled candidate S200114f

The GW candidate S200114f, an unmodelled transient trigger, occurred on 2020 January 14 02:08:18 UTC (LIGO Scientific Collaboration & Virgo Collaboration 2020e). The candidate was found by the Coherent Wave Burst analysis pipeline with a version of the search tagged as 'IMBH' (Klimenko et al. 2016; LIGO Scientific Collaboration & Virgo Collaboration 2020d). This event was observed by Virgo, LIGO-Livingston and LIGO-Hanford. Its

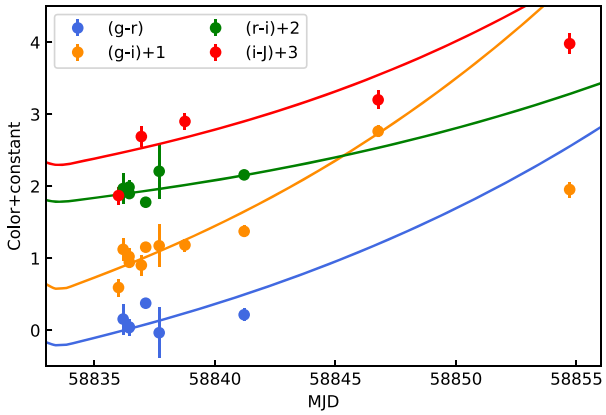

Figure 13. The colour evolution of AT 2019wxt. Note that the GW trigger time corresponds to MJD 58830.190. The circles correspond to the observed colours that are corrected for Galactic extinction. The solid lines correspond to the fitting results based on the Interaction model.

false alarm rate was about one in 25 yr. The 90 per cent credible region of the sky localization area is 403 deg^2; no further update on this trigger has been circulated to date. No distance estimate was provided. It is the only 'burst' alert transmitted during O3. By comparison, 5 'burst' alerts were sent during O2, but these triggers were either retracted or found to be consistent with noise (Abbott et al. 2019a). The event S200114f is interesting since none of the modelled search pipelines produced triggers during the same time period. Since no neutrinos (high or low energy) were recorded around the time of the trigger (Ageron & ANTARES Collaboration 2020; Colomer et al. 2020; IceCube Collaboration 2020a), a galactic SN is not likely to be the origin. If the event is astrophysical, a possible scenario for the GW emission is a massive BBH coalescence for which the inspiral phase is at too low of frequency and cannot be detected by LIGO and Virgo (Abbott et al. 2019d). A GW signal from a cosmic string is a more exotic possibility (Abbott et al. 2018b), as is GW emission from an unknown source (Abbott et al. 2019c).

Several teams followed the GW burst candidate S200114f and about 30 GCN circulars were sent. According to the follow-up observations, no neutrino events have been reported in spatial coincidence with S200114f by IceCube, which collected good quality data during the time the event occurred (IceCube Collaboration 2020a), or by ANTARES, which had only a 6.0 per cent chance that the GW source was in its FoV (Ageron & ANTARES Collaboration 2020); nor has any counterpart been reported by a gamma-ray space instrument, such as *Fermi*/LAT (Scotton, Longo & Fermi-LAT Collaboration 2020). SAGUARO observed 180 deg^2 of the S200114f sky localization area starting from 2.1 h after the trigger time with a typical limiting magnitude of 21. Five candidates were reported but they are unlikely to be related to the trigger. All of these are possibly variable stars or AGNs (Lundquist et al. 2020). *Swift* reported a possible X-ray transient source, S200114f-X2, which is coincident with a candidate AGN, and therefore this rise in flux may indicate nothing more than AGN activity and variability (Evans 2020a, b).

5.4.1 *GRANDMA observations*

Five GRANDMA telescopes participated in the follow-up of S200114f, as shown in Table 6, as soon as they received the GRANDMA observation plan (see Section 4). Time delays for FRAM between the first observation and the trigger time were

as follows: FRAM-Auger – 19 min, FRAM-CTA-N – 20 min; observations were obtained in the R_C filter. The TAROT network observed the most probable region about 15 h after the alert due to technical problems during the first night. The respective time delays are: TCA – 934 min, TRE – 901 min, TCH – 908 min; images were obtained without a filter. These observations covered about 77 per cent of the sky localization area in the following 90 h for a total sky coverage of 351 deg^2, as shown in Fig. A1 in Appendix A. Note that FRAM-Auger observed 28 per cent of the sky localization area in the first two hours after the GW trigger time for a total coverage of 20 deg^2. GRANDMA observations were reported in Corre et al. (2020) and no significant transient candidates were found with our low-latency analysis. We also conducted further analysis on our FRAM images on the two lists of ZTF candidates mentioned above. In particular, ZTF20aafemdh and ZTF20aafeogg were observed by FRAM-Auger 29 and 0.5 h before ZTF observations in $g'r'$ bands to a depth of 21 mag. We did not detect any point source at 5σ confidence in the R_C band to 16.2 mag. ZTF20aafemxx was also not detected to 16.2 mag in the R_C band by FRAM-CTA 1.5 h before the ZTF detection at 22 mag in the r' band.

5.5 The binary neutron star merger candidate S200213t

The GW candidate S200213t was identified on 2020 February 13 04:10:40.328 UTC (LIGO Scientific Collaboration & Virgo Collaboration 2020h). It is a three-detector trigger event, being observed by Virgo and both LIGO-Livingston and LIGO-Hanford. S200213t was reported to have a false-alarm rate of about one in 1 yr and 9 months. It has a non-negligible probability of 37 per cent to be a terrestrial artefact, whereas the probability of being a BNS is 63 per cent.

Nevertheless, assuming the candidate is astrophysical in origin, the probability of the presence of remnant matter is higher than 99 per cent. The first evaluation of the distance and the first estimate of 90 per cent credible sky localization area provided by the real time analysis (Kapadia et al. 2020) were 224 $\pm$ 90 Mpc and 2587 deg^2. These two quantities were updated three days later as follows (LIGO Scientific Collaboration & Virgo Collaboration 2020i): the luminosity distance is 201 $\pm$ 80 Mpc and the 90 per cent credible region to 2326 deg^2. The most updated sky localization using LALInference is shown in Fig. 14, both the full sky coverage and a zoomed-in panel.

Given the possible BNS nature of S200213t, the follow-up campaign performed by multiple groups was extensive, producing more than 50 GCNs. A muon neutrino candidate was detected by IceCube 175.94 s prior to GW trigger, which overlapped with the sky localization of S200213t (IceCube Collaboration 2020b). No gamma-ray transients were reported by *MAXI* (Kawai & MAXI Team 2020), *INTEGRAL* (Rodi et al. 2020), and Insight-*HXMT* (Zheng et al. 2020). *Swift*/BAT and Fermi were not in science mode (Sakamoto & Swift Team 2020; Cutini & Fermi-LAT Collaboration 2020; Veres, Fermi-GBM Team & GBM-LIGO/Virgo Group 2020). In the optical bands, galaxy targeted observations were performed by KAIT, observing 108 galaxies within the 90 per cent probability region (Vasylyev et al. 2020), J-Gem, observing a total of 37 galaxies (Kaneko & J-GEM Collaboration 2020), GECKO, observing four galaxies (Paek et al. 2020), and NAOC/CAS, observing 16 galaxies (Xu et al. 2020) compatible with the sky localization volume of S200213t. ZTF covered almost 80 per cent of the Bayestar sky localization area in one night to a magnitude limit of 21 mag in the $g'r'$ bands. ZTF also reported, in three different circulars (Kasliwal, ZTF Collaboration & GROWTH Collaboration 2020; Andreoni, ZTF Collaboration & GROWTH Collaboration 2020b; Reusch et al. 2020), a total of 15 candidates. ZTF provided a re-evaluation of the candidates after the delivery of an updated sky localization area, leaving seven candidates (Coughlin, ZTF Collaboration & GROWTH Collaboration 2020c). Bellm, Graham & GROWTH Collaboration (2020), Hu et al. (2020), De, ZTF Collaboration & GROWTH Collaboration (2020) showed that four of these candidates were unrelated to S200213t and offered some non-detection upper limits on a fifth candidate. MASTER also claimed a candidate in Lipunov et al. (2020a) and another one in Lipunov et al. (2020b). The last candidate was proven to be unrelated to S200213t by Mroz et al. (2020). DDOTI/OAN covered $\approx$50 per cent of the Bayestar sky localization area down to a limiting magnitude of 19.2 mag in the w band and less than an hour after the trigger time (Watson 2020). GOTO also immediately covered $\approx$54 per cent of the Bayestar sky localization area, down to a limiting magnitude of 18.4 mag in the L band (Cutter et al. 2020).

5.5.1 *GRANDMA observations*

The first notice was released 25 min after the trigger. Five wide FoV telescopes participated in the follow-up : TCA, TRE, OAJ, FRAM-CTA-N, FRAM-Auger, and TCH. At the time of the trigger, the FRAM network, TCA and TCH had the capacity to observe but due to bad weather or technical issues did not; OAJ requested to trigger the target of opportunity program, but it would not have been performed before the end of the night. Only TCA responded quickly to the alert. The first image was taken 26 min after the alert for TCA, 717 min for TRE, 898 min for OAJ, 932 min for FRAM-CTA-N (second night), 1220 min for FRAM-Auger (second night), and 2703 min for TCH (third night). These observations account for about 33 per cent of the cumulative probability of the LALInference sky localization area and are shown in Fig. 14. This sky localization area was covered by TCA in less than 24 h. No significant transient candidates were discovered (Blazek et al. 2020a).

The observational campaign was complemented with three days of optical follow-up from two 60 cm UBAI telescopes (UBAI-T60S and UBAI-T60N). The observations were performed in the galaxy targeting mode 6.7 d after the GW alert, with a delay due to bad weather conditions. We obtained photometric observations in the R_C filter reaching a limiting magnitude of 17 mag at 5σ confidence, using the list of fields provided for the most updated version of the sky localization area. The 16 fields observed contained a total of 47 galaxies observed by UBAI-T60N and 39 galaxies observed by UBAI-T60S, but no significant transient candidate was found. VIRT also observed two fields containing galaxies of interest located in the sky localization area starting at 2020 February 21 00:00:37, for example 188 h after the trigger time. The delay was due to poor weather conditions as well. The photometric analysis of the two fields gave an upper limit in the R_C band at 5σ confidence of 17 mag.

From the GRANDMA *kilonova-catcher* community, we obtained 34 images containing 29 galaxies localized in the 90 per cent C.L. sky localization area. The imaging latencies with respect to the GW trigger times were 0.91–4.96 d. We summarize the *kilonova-catcher* observations in Table B1. No optical transient was found at any galaxy position and constraints on their underlying optical flux were derived, resulting in unfiltered limiting magnitudes spanning $m_{\rm Lum} = 17.7 \pm 0.7$ mag at 5σ confidence.

No significant candidates were found by our initial analysis when crosschecking with databases of known objects or transients (see Section 4). GRANDMA also observed some interesting

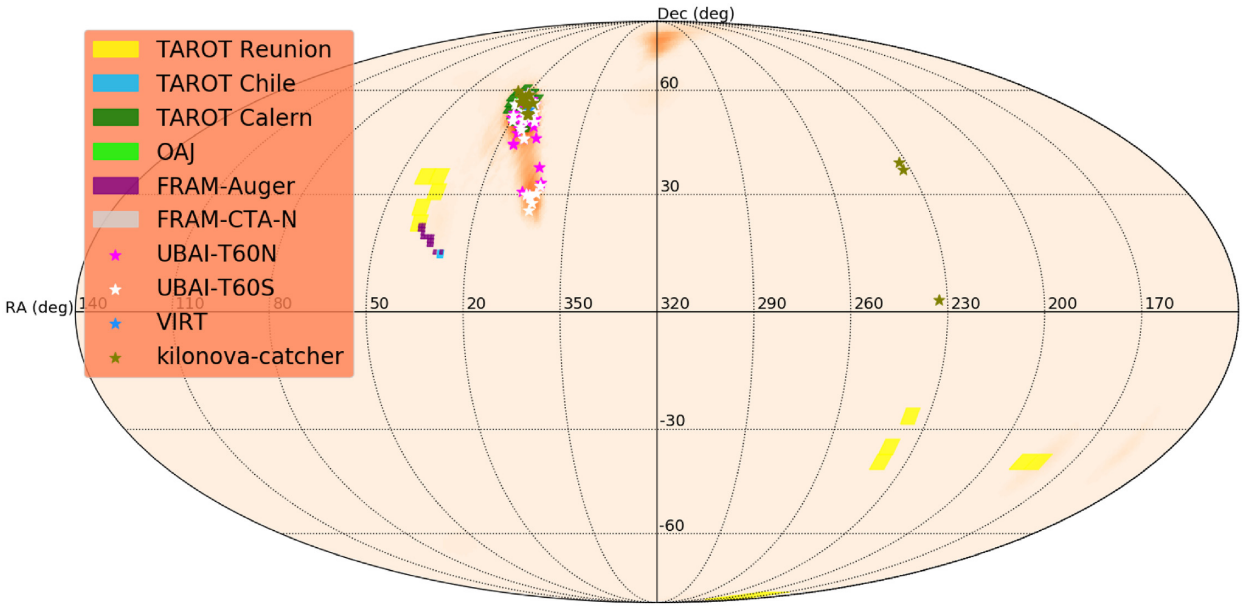

(a)

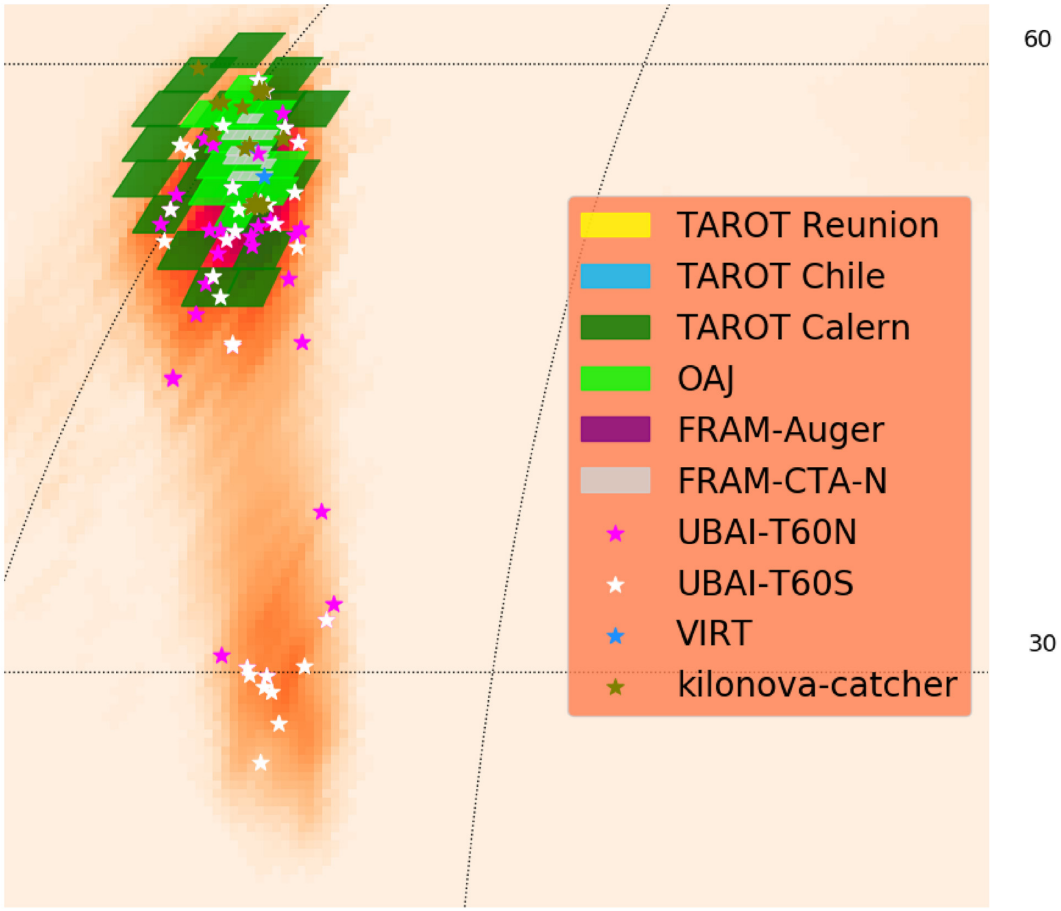

(b)

Figure 14. GRANDMA follow-up of the GW candidate S200213t, a BNS merger candidate. Yellow, blue, and dark green tiled areas represent observational tiles obtained by the TAROT network. Purple and grey tiled areas represent observational tiles obtained by the FRAM network. Light green tiled areas represent observational tiles obtained by OAJ. In red, the LALInference sky localization area of S200213t is shown. We note that TRE tiles covered 193 deg^2 yet only 1 per cent of the final sky area localization. Stars represent galaxy-targeting fields obtained by UBAI and VIRT (several days after the GW trigger time) and the citizen science program *kilonova-catcher* (with first images taken a few hours after the GW candidate trigger time).

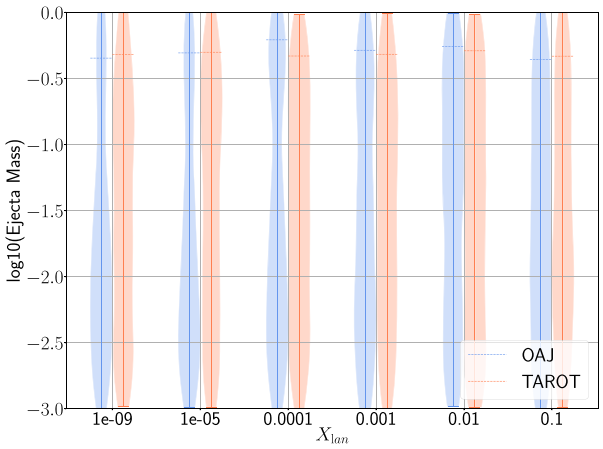

Figure 15. Constraints on the ejecta mass in terms of lanthanide fractions $X_{\rm lan}$ for the BNS candidate S200213t based on the OAJ and TAROT observations. The thickness of the vertical bands represents the probability density for this particular ejecta mass. Thick regions mark more probable regions of the parameter space, thin regions less probable ejecta masses. Overall, we find that for lower lanthanide fractions $X_{\rm lan}$ we are able to disfavour high ejecta masses, while for large lanthanide fractions no real constraints can be extracted. We mark the 90 per cent upper limits as horizontal dashed lines, where we clearly see that for most scenarios our upper bounds are reflecting the prior.

counterpart candidates mentioned above. The independent observations of GRANDMA covered most of the candidates presented in Kasliwal et al. (2020), Andreoni et al. (2020b), Reusch et al. (2020), and Lipunov et al. (2020b). For example, ZTF20aapvtip and ZTF20aamvoxx were observed by TAROT-Reunion but at a lower sensitivity and hours after ZTF. VIRT performed targeted observations of ZTF20aamvnth (AT2020cjb) and ZTF20aamvmzj (AT2020cja) and reported upper limits on the two sources: 17.8 mag (in the *Rc* band at 5σ confidence) in data taken from 2020 February 13 23:31:11 to 2020 February 14 00:46:03 and 17.8 mag (in the R_C band) on data taken from 2020 February 14 00:48:27 to 2020 February 14 01:11:05. Two months after the event, we conducted further analysis on OAJ observations with *Gmadet* (see Section 4). Among the $\sim$ 1800 transient candidates, we selected the most 200 promising events. We found an interesting transient which we classified as a moving object based on a near-in-time upper limit from the ZTF. However, the upper limits obtained with TAROT (with data taken the first night) and OAJ (with data taken the second night) can be used to constrain the ejecta properties of potential kilonova that may have occurred in the vicinity of the observed galaxies. These are described in more details in the following Section 5.5.2.

5.5.2 Constraining kilonova properties

We seek now to derive constraints on the observed GW transients from GRANDMA observations. As an example, we will focus in particular on the BNS candidate S200213t. Within the GRANDMA network, a number of telescopes searched for a kilonova counterpart to this event, among these OAJ which covered part of the sky localization area to a magnitude $r' > 20.1$ mag (at 5σ detection level),TAROT to a limiting magnitude of $CR > 18$ mag, and a number of individual galaxy-targeted searches that also reached limiting magnitudes around 18 mag (see Table B1 in the Appendix B). Under the assumption that TAROT (which achieved 30 per cent coverage of the relevant sky area) or OAJ (which achieved 18 per cent coverage of the relevant sky area) covered the relevant sky location, we derive constraints on the ejecta mass consistent with the non-detection of any kilonova.

For a quantitative interpretation, we follow Antier et al. (2020) and Coughlin et al. (2020b), we derive generic ejecta masses $M_{\rm ej}$, ejecta velocities $v_{\rm ej}$, and lanthanide fractions $X_{\rm lan}$ that are consistent with the non-observation of a counterpart in our observational searches. Fig. 15 summarizes our results. Unfortunately, independent of the lanthanide fraction of the ejected material, we are not able to derive a constraint on the ejecta mass. Even very large ejecta masses of the order of $\sim$0.4 $M_\odot$, that are typically disfavoured by numerical-relativity simulations (Dietrich & Ujevic 2017), cannot be ruled out. For comparison, the ejecta mass of GW170817 is estimated to be $\sim$0.05 $M_\odot$, that is about one order of magnitude smaller. Furthermore, the exact 90 per cent upper bound on the ejecta mass (vertical lines in Fig. 15) seems to be prior-dominated, which is another indicator that no reliable information can be extracted. Therefore, it seems likely that just from our observations, sources compatible to GW170817 would have been missed due to the significantly larger distance of S200213t, $\sim$5 times further away.

6 CONCLUSIONS

In conclusion, the coordination of joint observations across a telescope network, above and beyond just recording independent observations from various groups, is an important goal for deriving multimessenger science with EM and GW data. Within GRANDMA, we have performed such joint observations whereby we obtain a combination of repeated and split observations over the telescopes in our network, including scheduling them to perform observations in different bands at different times in order to make it possible to potentially determine colour and luminosity evolution of any transients that we might discover. GRANDMA has demonstrated the coordination of observations from a very diverse array of facilities; it has also achieved significant success in terms of coverage of the GW sky localization areas in a variety of bands and to a variety of limiting magnitudes. In this paper, we particularly focused on the second part of O3 and the two BNS merger candidates S191213g and S200213t. While we derived constraints on potential kilonova properties of S200213t, thanks to the active follow-up by six wide FoV telescopes of the network, we also targeted follow-up of a candidate optical counterpart which turned out to be a Type IIb SN with possible evidence of CSM interaction.

GRANDMA has followed-up about 90 per cent of the GW alerts during O3, covering about 50 events, including BBHs, to demonstrate our global coordination system. GRANDMA is composed of 25 telescopes inspired to contribute to this global effort, and remains a flexible and open collaboration. We have also highlighted the GRANDMA's unique citizen science program, involving, for the first time, amateur astronomers following-up potential GW events. Given the number of GW triggers, optical transients, and the necessary data reduction procedures, such a collaboration needs dedicated human organization, data analysis, and protocol communication to manage targets of observations obtained by many different telescopes. In this sense, GRANDMA is well prepared for the next GW observing run O4 with possible rates of one transient per day.

ACKNOWLEDGEMENTS

Parts of this research were conducted by the Australian Research Council Centre of Excellence for Gravitational Wave Discovery (OzGrav), through project number CE170100004.

EJH acknowledges support from an Australian Research Council DECRA Fellowship (DE170100891). AdUP and CCT acknowledge support from Ramón y Cajal fellowships RyC-2012-09975 and RyC-2012-09984 and the Spanish Ministry of Economy and Competitiveness through project AYA2017-89384-P. DAK acknowledges Spanish research project RTI2018-098104-J-I00 (GRBPhot). MB acknowledges funding as 'personal tecnico de apoyo' under fellowship number PTA2016-13192-I. SA is supported by the CNES Postdoctoral Fellowship at Laboratoire AstroParticule et Cosmologie. SA and CL acknowledge the financial support of the Programme National Hautes Energies (PNHE). DT acknowledges the financial support of CNES postdoctoral program. UBAI acknowledges support from the Ministry of Innovative Development through projects FA-Atech-2018-392 and VA-FA-F-2-010. SB acknowledges Shota Rustaveli National Science Foundation (SRNSF) grant no. – PHDF/18-1327. TAROT has been built with the support of the Institut National des Sciences de l'Univers, CNRS, France. TAROT is funded by the CNES and thanks the help of the technical staff of the Observatoire de Haute Provence, OSU-Pytheas. MP, SK, and MM are supported by European Structural and Investment Fund and the Czech Ministry of Education, Youth and Sports (Projects CZ.02.1.01/0.0/0.0/16_013/0001402, CZ.02.1.01/0.0/0.0/16_013/0001403, and CZ.02.1.01/0.0/0.0/15_003/0000437). NBO, DM, and PG acknowledge financial support from NASA-MUREP-MIRO grant NNX15AP95A, NASA-EPSCoR grant NNX13AD28A, and NSF EiR AST Award 1901296. The GRANDMA collaboration thank the amateur participants to the *kilonova-catcher* program. The *kilonova-catcher* program is supported by the IdEx Université de Paris, ANR-18-IDEX-0001. This research made use of the crossmatch service provided by CDS, Strasbourg. We thank Ulrich Hopp to provide the precise date of observations for AT2019wxt Wendelstein optical observations.

DATA AVAILABILITY

The data underlying this article will be shared on reasonable request to the corresponding author.

REFERENCES

Aasi et al., 2015, Class. Quantum Gravity, 32, 074001
Abbott B. P. et al., 2016, Phys. Rev. Lett., 116, 221101
Abbott B. P. et al., 2017a, Phys. Rev. Lett., 119, 161101
Abbott B. P. et al., 2017b, ApJ, 848, L12
Abbott B. P. et al., 2018a, Living Rev. Relativ., 21, 3
Abbott B. P. et al., 2018b, Phys. Rev., D97, 102002
Abbott B. P. et al., 2019a, ApJ, 875, 161
Abbott B. P. et al., 2019b, ApJ, 882, L24
Abbott B. P. et al., 2019c, Phys. Rev., D100, 024017
Abbott B. P. et al., 2019d, Phys. Rev., D100, 064064
Abbott B. P. et al., 2019e, Phys. Rev. X, 9, 031040
Abbott B. P. et al., 2020, ApJ, 892, L3
Acernese et al., 2015, Class. Quantum Gravity, 32, 024001
Ackley K. et al., 2020, preprint (arXiv:2002.01950)
Ageron M., ANTARES Collaboration, 2020, GCN Circ., 26742, 1
Ageron M., Baret B., Coleiro A., Colomer M., Dornic D., Kouchner A., Pradier T., ANTARES Collaboration, 2019, GCN Circ., 26404, 1
Almualla M., Coughlin M. W., Anand S., Alqassimi K., Guessoum N., Singer L. P., 2020, MNRAS, 495, 4366
Alvarez-Muniz J., Pedreira F., Zas E., Kampert K. H., Schimp M., Pierre Auger Collaboration, 2019, GCN Circ., 26423, 1
Andreoni I. et al., 2019, GCN Circ., 26424, 1
Andreoni I. et al., 2020a, ApJ, 890, 131
Andreoni I., ZTF Collaboration, GROWTH Collaboration, 2020b, GCN Circ., 27065, 1
Antier S. et al., 2020, MNRAS, 492, 3904
Arcavi I., 2018, ApJ, 855, L23
Barthelmy S. D. et al., 2019, GCN Circ., 26410, 1
Barynova K. et al., 2019, GCN Circ., 26215, 1
Becker A., 2015, Astrophysics Source Code Library, record ascl:1504.004
Bellm E. C., Graham M., GROWTH Collaboration, 2020, GCN Circ., 27118, 1
Beradze S. et al., 2019, GCN Circ., 26362, 1
Berthier J., Vachier F., Thuillot W., Fernique P., Ochsenbein F., Genova F., Lainey V., Arlot J. E., 2006, SkyBoT, A New VO Service to Identify Solar System Objects. Astron. Soc. Pac., San Francisco, p. 367
Bhirombhakdi K., Chornock R., Miller A. A., Filippenko A. V., Cenko S. B., Smith N., 2019, MNRAS, 488, 3783
Blazek M. et al., 2020a, GCN Circ., 27116, 1
Blazek M. et al., 2020b, GCN Circ., 27168, 1
Blazek M. et al., 2020c, GCN Circ., 27409, 1
Bloemen S. et al., 2016, in Hall H. J., Gilmozzi R., Marshall H. K., eds, Proc. SPIE Vol. 9906, Ground-based and Airborne Telescopes VI. SPIE, Bellingham, p. 2118
Brunn S. H. et al., 2019, GCN Circ., 25384, 1
Casentini C. et al., 2019, GCN Circ., 26408, 1
Chambers K. C. et al., 2016, preprint (arXiv:1612.05560)
Chatterjee D., Ghosh S., Brady P. R., Kapadia S. J., Miller A. L., Nissanke S., Pannarale F., 2019, ApJ, 896, 54
Chatzopoulos E., Wheeler J. C., Vinko J., 2012, ApJ, 746, 121
Chatzopoulos E., Wheeler J. C., Vinko J., Horvath Z. L., Nagy A., 2013, ApJ, 773, 76
Christensen N. et al., 2019, GCN Circ., 26219, 1
Colomer M., Lincetto M., Coleiro A., Dornic D., Kulikovskiy V., KM3NeT Collaboration, 2020, GCN Circ., 26751, 1
Corre D. et al., 2020, GCN Circ., 26875, 1
Coughlin M. W. et al., 2018a, MNRAS, 478, 692
Coughlin M. W. et al., 2018b, MNRAS, 480, 3871
Coughlin M. W. et al., 2019a, MNRAS, 489, 5775
Coughlin M. W., Dietrich T., Margalit B., Metzger B. D., 2019b, MNRAS, 489, L91
Coughlin M. W. et al., 2019c, ApJ, 885, L19
Coughlin M. W. et al., 2020a, Phys. Rev. Res., 2, 022006
Coughlin M. W. et al., 2020b, MNRAS, 492, 863
Coughlin M., ZTF Collaboration, GROWTH Collaboration, 2020c, GCN Circ., 27095, 1
Coulter D. A. et al., 2017, Science, 358, 1556
Cutini S., Fermi-LAT Collaboration, 2020, GCN Circ., 27062, 1
Cutini S., Omodei N., Axelsson M., Bissaldi E., Kocevski D., Longo F., Arimoto M., Fermi-LAT Collaboration, 2019, GCN Circ., 26412, 1
Cutter R. et al., 2020, GCN Circ., 27069, 1
D'Avanzo P. et al., 2019, GCN Circ., 26499, 1
De K., ZTF Collaboration, GROWTH Collaboration, 2020, GCN Circ., 27140, 1
Dhillon V. S. et al., 2014, MNRAS, 444, 4009
Dichiara S. et al., 2019, GCN Circ., 26517, 1
Dietrich T., Ujevic M., 2017, Class. Quantum Gravity, 34, 105014
Doctor Z., Farr B., Holz D. E., Pürrer M., 2017, Phys. Rev. D, 96, 123011
Ducoin J. G. et al., 2019a, GCN Circ., 26384, 1
Ducoin J. G. et al., 2019b, GCN Circ., 26558, 1
Ducoin J. G. et al., 2019c, GCN Circ., 26575, 1
Ducoin J. G., Corre D., Leroy N., Le Floch E., 2020a, MNRAS, 492, 4768
Ducoin J. G. et al., 2020b, GCN Circ., 27275, 1
Ducoin J.-G. et al., 2020c, GCN Circ., 27322, 1
Duverne P. A. et al., 2019a, GCN Circ., 26469, 1
Duverne P. A. et al., 2019b, GCN Circ., 26528, 1
Evans P. A., 2020a, GCN Circ., 26787, 1
Evans P. A., 2020b, GCN Circ., 26791, 1
Flewelling H. A. et al., 2016, preprint (arXiv:1612.05243)

Fremling C., Kasliwal M., Perley D. A., Walters R., 2019, GCN Circ., 26500, 1
Ghirlanda G. et al., 2019, Science, 363, 968
Goldstein A. et al., 2017, ApJ, 848, L14
Goldstein D. A. et al., 2019, ApJ, 881, L7
Gotz D., Lutovinov A., Savchenko V., Ferrigno C., Rodi J., Coleiro A., Mereghetti S., INTEGRAL Multi-MESSENGER Collaboration, 2019, GCN Circ., 26401, 1
Hello P. et al., 2020, GCN Circ., 26789, 1
Herner K. et al., 2017, J. Phys.: Conf. Ser., 898, 032050
Hopp U., Kluge M., Goessl C., Ries C., Schmidt M., 2019, GCN Circ., 27057, 1
Hosseinzadeh G. et al., 2019, ApJ, 880, L4
Howell E. et al., 2020, GCN Circ., 27054, 1
Hu Y. D. et al., 2020, GCN Circ., 27154, 1
Huang F., Li J.-Z., Wang X.-F., Shang R.-C., Zhang T.-M., Hu J.-Y., Qiu Y.-L., Jiang X.-J., 2012, Res. Astron. Astrophys., 12, 1585
Huber M. E. et al., 2019, GCN Circ., 26577, 1
IceCube Collaboration, 2019, GCN Circ., 26399, 1
IceCube Collaboration, 2020a, GCN Circ., 26732, 1
IceCube Collaboration, 2020b, GCN Circ., 27043, 1
Izzo L. et al., 2019, GCN Circ., 26491, 1
Janeček P. et al., 2019, EPJ Web Conf., 197, 02008
Kaneko A., J-GEM Collaboration, 2020, GCN Circ., 27066, 1
Kapadia S. J. et al., 2020, Class. Quantum Gravity, 37, 045007
Kasen D., Metzger B., Barnes J., Quataert E., Ramirez-Ruiz E., 2017, Nature, 551, 80
Kasliwal M. M. et al., 2019, PASP, 131, 038003
Kasliwal M. M., ZTF Collaboration, GROWTH Collaboration, 2020, GCN Circ., 27051, 1
Kawai N., MAXI Team, 2020, GCN Circ., 27048, 1
Klimenko S. et al., 2016, Phys. Rev. D, 93, 042004
Kong A., Tan H., Ngeow C., Ip W., 2019, GCN Circ., 26503, 1
Lattimer J. M., Schramm D. N., 1974, ApJ, 192, L145
LIGO Scientific Collaboration, Virgo Collaboration, 2019a, GCN Circ., 24045, 1
LIGO Scientific Collaboration, Virgo Collaboration, 2019b, GCN Circ., 24237, 1
LIGO Scientific Collaboration, Virgo Collaboration, 2019c, GCN Circ., 24448, 1
LIGO Scientific Collaboration, Virgo Collaboration, 2019d, GCN Circ., 24717, 1
LIGO Scientific Collaboration, Virgo Collaboration, 2019e, GCN Circ., 25094, 1
LIGO Scientific Collaboration, Virgo Collaboration, 2019f, GCN Circ., 25138, 1
LIGO Scientific Collaboration, Virgo Collaboration, 2019g, GCN Circ., 25164, 1
LIGO Scientific Collaboration, Virgo Collaboration, 2019h, GCN Circ., 25187, 1
LIGO Scientific Collaboration, Virgo Collaboration, 2019i, GCN Circ., 25208, 1
LIGO Scientific Collaboration, Virgo Collaboration, 2019j, GCN Circ., 25324, 1
LIGO Scientific Collaboration, Virgo Collaboration, 2019k, GCN Circ., 25333, 1
LIGO Scientific Collaboration, Virgo Collaboration, 2019l, GCN Circ., 25549, 1
LIGO Scientific Collaboration, Virgo Collaboration, 2019m, GCN Circ., 25861, 1
LIGO Scientific Collaboration, Virgo Collaboration, 2019n, GCN Circ., 26182, 1
LIGO Scientific Collaboration, Virgo Collaboration, 2019o, GCN Circ., 26402, 1
LIGO Scientific Collaboration, Virgo Collaboration, 2019p, GCN Circ., 26413, 1
LIGO Scientific Collaboration, Virgo Collaboration, 2019q, GCN Circ., 26417, 1
LIGO Scientific Collaboration, Virgo Collaboration, 2019r, GCN Circ., 26417, 1
LIGO Scientific Collaboration, Virgo Collaboration, 2020a, GCN Circ., 26640, 1
LIGO Scientific Collaboration, Virgo Collaboration, 2020b, GCN Circ., 26665, 1
LIGO Scientific Collaboration, Virgo Collaboration, 2020c, GCN Circ., 26688, 1
LIGO Scientific Collaboration, Virgo Collaboration, 2020d, GCN Circ., 26734, 1
LIGO Scientific Collaboration, Virgo Collaboration, 2020e, GCN Circ., 26734, 1
LIGO Scientific Collaboration, Virgo Collaboration, 2020f, GCN Circ., 26785, 1
LIGO Scientific Collaboration, Virgo Collaboration, 2020g, GCN Circ., 27036, 1
LIGO Scientific Collaboration, Virgo Collaboration, 2020h, GCN Circ., 27042, 1
LIGO Scientific Collaboration, Virgo Collaboration, 2020i, GCN Circ., 27096, 1
LIGO Scientific Collaboration, Virgo Collaboration, 2020j, GCN Circ., 27130, 1
LIGO Scientific Collaboration, Virgo Collaboration, 2020k, GCN Circ., 27229, 1
Li L.-X., Paczynski B., 1998, ApJ, 507, L59
Lim G. et al., 2019, GCN Circ., 26520, 1
Lipunov V. et al., 2010, Adv. Astron., 2010, 349171
Lipunov V. et al., 2020a, GCN Circ., 27072, 1
Lipunov V. et al., 2020b, GCN Circ., 27077, 1
LSST Science Collaboration, 2009, preprint (arXiv:0912.0201)
Lundquist M. J. et al., 2019, GCN Circ., 26473, 1
Lundquist M. J. et al., 2020, GCN Circ., 26753, 1
Marrocchesi P. S. et al., 2019, GCN Circ., 26419, 1
McBrien O. et al., 2019, GCN Circ., 26485, 1
Metzger B. D., 2019, Living Rev. Relativ., 23, 1
Metzger B. D., Bauswein A., Goriely S., Kasen D., 2015, MNRAS, 446, 1115
Mooley K. P. et al., 2018, Nature, 554, 207
Mroz P., Gromadzki M., Udalski A., OGLE Team, 2020, GCN Circ., 27085, 1
Muthukrishna D., Narayan G., Mandel K. S., Biswas R., Hložek R., 2019, PASP, 131, 118002
Noysena K., Klotz A., Boër M., Laugier R., Komonjinda S., Turpin D., The TAROT Collaboration, 2019, ApJ, 886, 73
Noysena K. et al., 2020, GCN Circ., 26820, 1
O'Brien P., 2018, in 42nd COSPAR Scientific Assembly. ESA online, p. E1.15–18-18
Oates S. R. et al., 2019, GCN Circ., 26501, 1
Paek G. S. H. et al., 2020, GCN Circ., 27067, 1
Prouza M., Jelínek M., Kubánek P., Ebr J., Trávníček P., Šmída R., 2010, Adv. Astron., 2010, 849382
Reusch S., Stein R., Perley D., Anand S., ZTF Collaboration, GROWTH Collaboration, 2020, GCN Circ., 27068, 1
Rodi J., Savchenko V., Ferrigno C., Coleiro A., Mereghetti S., INTEGRAL Multi-Messenger Collaboration, 2020, GCN Circ., 27050, 1
Sadibekova T. et al., 2019, GCN Circ., 26361, 1
Sadibekova T. et al., 2020, GCN Circ., 27238, 1
Sakamoto T., Swift Team, 2020, GCN Circ., 27058, 1
Salmaso I. et al., 2019, GCN Circ., 25650, 1
Savchenko V. et al., 2017, ApJ, 848, L15
Scotton L., Longo F., Fermi-LAT Collaboration, 2020, GCN Circ., 26745, 1
Shenoy V., Aarthy E., Bhalerao V., Bhattacharya D., Rao A. R., Vadawale S., AstroSat CZTI Collaboration, 2019, GCN Circ., 26425, 1
Singer L. P., Price L. R., 2016, Phys. Rev. D, 93, 024013
Smith N., 2014, ARA&A, 52, 487
Stachie C. et al., 2020a, GCN Circ., 26947, 1
Stachie C., Coughlin M. W., Christensen N., Muthukrishna D., 2020b, MNRAS, in press

Stein R., Reusch S., Perley D., Andreoni I., Coughlin M., ZTF Collaboration, GROWTH Collaboration, 2019, GCN Circ., 26437, 1
Sugita S. et al., 2019, GCN Circ., 26403, 1
Sun T. et al., 2019, GCN Circ., 26510, 1
Tonry J. L., 2011, PASP, 123, 58
Turpin D. et al., 2020, GCN Circ., 26687, 1
Vallely P. et al., 2019, GCN Circ., 26508, 1
Vasylyev S., Sunseri J., Girish N., Murakami Y., Zheng W., Filippenko A. V., Lick/KAIT GW Follow-Up Team, 2020, GCN Circ., 27064, 1
Veitch J. et al., 2015, Phys. Rev. D, 91, 042003
Veres P., Fermi-GBM Team, GBM-LIGO/Virgo Group, 2020, GCN Circ., 27056, 1
Verrecchia F. et al., 2019, GCN Circ., 26407, 1
Vogl C. et al., 2019, GCN Circ., 26504, 1
Wang X. et al., 2008, ApJ, 675, 626
Wang L. J. et al., 2019, MNRAS, 489, 1110
Watson A. M., 2020, GCN Circ., 27061, 1
Watson A. M. et al., 2020, MNRAS, 492, 5916
Wilson-Hodge C. A., Fermi-GBM Team, GBM-LIGO/Virgo Group, 2019, GCN Circ., 26409, 1
Wyatt S. D., Tohuvavohu A., Arcavi I., Lundquist M. J., Howell D. A., Sand D. J., 2020, ApJ, 894, 127
Xiao S. et al., 2019, GCN Circ., 26433, 1
Xin L. P., SVOM Multi Messenger Astronomy Team, GWAC Team, 2020, GCN Circ., 26948, 1
Xu D. et al., 2020, GCN Circ., 27070, 1
York D. G. et al., 2000, AJ, 120, 1579
Zackay B., Venumadhav T., Dai L., Roulet J., Zaldarriaga M., 2019, Phys. Rev. D, 100, 023007
Zheng Y. G. et al., 2020, GCN Circ., 27071, 1
Zhu Z. P. et al., 2019, GCN Circ., 26488, 1

SUPPORTING INFORMATION

Supplementary data are available at *MNRAS* online.

GRANDMA_O3b_final_appendix.pdf

Please note: Oxford University Press is not responsible for the content or functionality of any supporting materials supplied by the authors. Any queries (other than missing material) should be directed to the corresponding author for the article.

[1]*CNRS, Astroparticule et Cosmologie, Université de Paris, F-75013 Paris, France*
[2]*N. Tusi Shamakhy Astrophysical Observatory Azerbaijan National Academy of Sciences, settl.Mamedaliyev, AZ 5626, Shamakhy, Azerbaijan*
[3]*Physics Department, American University of Sharjah, P.O. Box 26666, Sharjah, UAE*
[4]*National Astronomical Research Institute of Thailand, 260, Moo 4, T. Donkaew, A. Mae Rim, Chiang Mai 50180, Thailand*
[5]*Astronomical Observatory Taras Shevshenko National University of Kyiv, Observatorna str. 3, Kyiv 04053, Ukraine*
[6]*Nuclear Physics Department Taras Shevchenko National University of Kyiv, 60 Volodymyrska str., Kyiv 01601, Ukraine*
[7]*E. Kharadze Georgian National Astrophysical Observatory, Mt.Kanobili, Abastumani, 0301 Adigeni, Georgia*
[8]*Samtskhe-Javakheti State University, Rustaveli Str. 113, Akhaltsikhe, 0080 Georgia*
[9]*Instituto de Astrofísica de Andalucía (IAA-CSIC), Glorieta de la Astronomía s/n, E-18008 Granada, Spain*
[10]*ARTEMIS UMR 7250 UCA CNRS OCA, Boulevard de l'Observatoire, CS 34229, F-06304 Nice CEDEX 04, France*
[11]*Ulugh Beg Astronomical Institute, Uzbekistan Academy of Sciences, Astronomy str. 33, Tashkent 100052, Uzbekistan*
[12]*IJCLab, Univ Paris-Saclay, CNRS/IN2P3, F-91898 Orsay, France*
[13]*School of Physics and Astronomy, University of Minnesota, Minneapolis, MN 55455, USA*
[14]*School of Physics, OzGrav-UWA, University of Western Australia, M013, 35 Stirling Highway, Crawley, WA 6009, Australia*
[15]*Institut für Physik und Astronomie, Universität Potsdam, Haus 28, Karl-Liebknecht-Str. 24/25, D-14476 Potsdam, Germany*
[16]*University of the Virgin Islands, College of Science and Math, 2 John Brewer's Bay, St. Thomas, VI 00802, USA*
[17]*Volkssternwarte Paderborn e.V. Im Schlosspark 13, D-33104 Paderborn – Schloss Neuhaus, Germany*
[18]*FZU – Institute of Physics of the Czech Academy of Sciences, Prague, Czech Republic*
[19]*IRAP, Université de Toulouse, CNRS, UPS, 14 Avenue Edouard Belin, F-31400 Toulouse, France*
[20]*Université Paul Sabatier Toulouse III, Université de Toulouse, 118 route de Narbonne, F-31400 Toulouse, France*
[21]*Physics Department and Astronomy Department, Tsinghua University, Beijing 100084, China*
[22]*OrangeWave Innovative Science, LLC, Moncks Corner, SC 29461, USA*
[23]*Department of Physics and Materials Science, Faculty of Science, Chiang Mai University, Chiang Mai 50200, Thailand*
[24]*CNRS, CEA, Département d'Astrophysique, Astrophysique, Instrumentation et Modélisation de Paris-Saclay, Université Paris-Saclay, F-91191 Gif-sur-Yvette, France*
[25]*Astronomy and Space Physics Department, Taras Shevchenko National University of Kyiv, 60 Volodymyrska str., Kyiv 01601, Ukraine*
[26]*National University of Uzbekistan, 4 University str., Tashkent 100174, Uzbekistan*
[27]*Laboratoire d'Annecy de Physique des Particules (LAPP), Univ. Grenoble Alpes, Université Savoie Mont Blanc, CNRS/IN2P3, F-74941 Annecy, France*
[28]*Yunnan Astronomical Observatories/Chinese Academy of Science, Kunming 650011, China*
[29]*National Astronomical Observatories/Chinese Academy of Science 20A Datun Road, Beijing 100012, China*

This paper has been typeset from a TEX/LATEX file prepared by the author.